STREAMFLOW VARIABILITY UNDER CLIMATE CHANGE SCENARIOS IN KELANI RIVER BASIN, SRI LANKA

Farid Farhat

208350M

Degree of Master of Science

Department of Civil Engineering

University of Moratuwa
Sri Lanka

February 2022

STREAMFLOW VARIABILITY UNDER CLIMATE CHANGE SCENARIOS IN KELANI RIVER BASIN, SRI LANKA

Farid Farhat

208350M

Supervised by
Dr R. M. J. Bamunawala
and
Dr T. M. N. Wijayaratna

Thesis submitted in partial fulfillment of the requirements for the degree
Master of Science in Civil Engineering

UNESCO Madanjeet Singh Centre for
South Asia Water Management (UMCSAWM)
Department of Civil Engineering

University of Moratuwa
Sri Lanka

February 2022

DECLARATION OF THE CANDIDATE AND SUPERVISOR

"I declare that this is my own work and this thesis does not incorporate without acknowledgement any material previously submitted for a Degree or Diploma in any other University or institute of higher learning and to the best of my knowledge and belief it does not contain any material previously published or written by another person except where the acknowledgement is made in the text".

Also, I hereby grant to University of Moratuwa the non-exclusive right to reproduce and distribute my thesis/dissertation, in whole or in part in print, electronic or other medium. I retain the right to use this content in whole or part in future works (such as articles or books).

UOM Verified Signature

29-Apr-2022

Farid Farhat

Date

The above candidate has carried out research for the Masters thesis under my supervision

UOM Verified Signature

29-Apr-2022

-- ----------------------------

Dr R. M. J. Bamunawala

Date

UOM Verified Signature

29-Apr-2022

Dr T. M. N. Wijayaratna

Date

ABSTRACT

Streamflow Variability under Climate Change Scenarios in Kelani River Basin, Sri Lanka

In recent years, the downstream floodplain of the Kelani River Basin has been suffering from frequent floods. With the current climate change trend, flood-related damages are expected to amplify in future. Therefore, understanding how such extreme events behave in the future is quite essential for the basin planners and managers. Using the output from three global climate models (CNRM-CM6-1, MRI-ESM2-0, EC-Earth3-CC, and their ensemble) from the Sixth Phase of Coupled Model Intercomparison Project (CMIP6), variation of streamflow was evaluated from historical (1985-2014) to mid-century (2030-2059) and late-century (2070-2100) periods under Shared Socioeconomic Pathways (SSPs 2-4.5 and 5-8.5). Bias-corrected precipitation and temperature through linear scaling and power transformation, respectively were fed into the HEC-HMS model to project future river discharge. Based on the ensemble model, changes in average annual discharge indicates an increasing trend in future periods under both scenarios considered. Significantly high changes were projected in the late century (25-40 m^3/s) compared to the mid-century (15-25 m^3/s) under both scenarios. Projected changes in monthly streamflow indicate an increasing trend for wet months (June-December) while a decreasing trend for dry months (January-May). Further, the highest changes in streamflow were identified in the monthly changes (-5 to 60 and -5 to 100 m^3/s under SSP2-4.5 and SSP5-8.5, respectively). Comparison of seasonal changes shows the highest increase for Southwest Monsoon (40-60 m^3/s under both scenarios and future periods) while the highest decrease for First-Inter monsoon (<-10 m^3/s under both scenarios and future periods). Moreover, changes in high, median, and low flows (5%, 50%, and 95% percentiles of flow duration curve, respectively) indicate significant changes in high flows compared to the median and low flows. The findings of this study suggest a significant increase in high flows during the Southwest Monsoon that can further threaten the basin with the devastating floods. The results provide important insight for planners and other stakeholders dealing with water resources management in the basin.

Keywords: Streamflow Changes, Climate Change Impact, Shared Socioeconomic Pathway

DEDICATION

My work is dedicated to my dear

Mother and Uncles

Whose affection, love, encouragement, and financial support of each day and night allowed me to accomplish my dreaming master's degree. With my best wishes, I hope a successful and happy life for you all

ACKNOWLEDGEMENT

Herewith, I would like to convey my sincere gratitude to Dr. R. M. J. Bamunawala, who supervised my work and guided me during the entire process. Working with him was a once-in-life-time opportunity for me. Dr. Bamunawala was not only supportive for the academic workload at any time, but he was also an outstanding motivator in my personal life. His friendly, flexible, and collaborative attitude were among the many of his assets that makes working with him truly enjoyable. The success of this research is mainly attributed to his valuable contribution.

The author also would like to extend his gratitude to the UMCSAWM Director, Professor R. L. H. Rajapakse for his invaluable feedback and many other supports. He was a rich and insightful academic source for me and all my fellows that shaped our research. It was his hard work and time management that lead to the completion of our program during the challenging time of the COVID pandemic.

I would like to thank my mentor, Mr. H.W. Kumarasinghe for his kind assistance during my stay in Sri Lanka. Frankly speaking, he was always there when we had any problem, which made him like a real father. Additionally, I feel honoured to extend my gratitude to all members of the UMCSAWM and Department of Civil Engineering for their support through any means. Finally, my sincere thanks go to the South Asia Foundation for providing me with a fully funded scholarship to achieve my master's degree.

TABLE OF CONTENTS

LIST OF FIGURES

LIST OF TABLES

LIST OF ABBREVIATIONS

AR	Assessment Report
CDS	Climate Data Store
CMIP	Coupled Model Intercomparison Project
CMhyd	Climate Model for Hydrologic Modelling
ESGF	Earth System Grid Federation
GCM	Global Climate Model
IAM	Integrated Assessment Model
IAV	Impact Adaption Vulnerability
IPCC	Intergovernmental Panel on Climate Change
KRB	Kelani River Basin
RCM	Regional Climate Model
RCP	Representative Concentration Pathway
SSP	Shared Socioeconomic Pathway
WGCM	Working Group of Coupled Modelling
WRCP	World Climate Research Program

CHAPTER 1

1 RESEARCH BACKGROUND

This chapter provides a comprehensive introduction and scope of the research. Its contents include the introduction of the research, problem statement, main and specific objectives. The chapter addresses research problem and provides details on how the issues are addressed through main and specific objectives.

1.1 Introduction

Earth's climate system has been experiencing significant change in recent years (Gunathilake et al., 2020). Increased industrialization and urbanization, alarming population growth, coupled with unsustainable practices, and use of fossil fuels are major contributors to the change in the climate system (Shrestha et al., 2013; Bajracharya, et al., 2016; Stocker et al., 2013). Among the many consequences of climate change, rising temperature is the most notable change that impacts the natural systems and society (Bhatta et al., 2019) . The planet is becoming warmer and by the end of the 21st century, the global surface temperature is expected to exceed by 1.5 °C relative to 1850–1900 for all RCP scenarios except RCP 2.6 (Stocker et al., 2013). The temperature change can significantly influence the hydrologic cycle because two major components of the water cycle, precipitation and evapotranspiration, are governed by its variation (Gunathilake et al., 2020). This will have a profound impact on streamflow variation on a catchment scale.

Furthermore, assessment of sediment transport and streamflow from Gorganroud watershed in North of Iran, Koshi basin in Nepal, Nam Ou basin in Los, and Changling watershed in Northeast China indicate sediment transport and discharge increase under most of climate change scenario (Azari et al., 2016; Devkota & Gyawali, 2015; Shrestha et al., 2013; Zhou et al., 2017). The higher variation in streamflow due to climate change will lead to numerous challenges in a basin. Flood and droughts will become more severe as the timing and magnitude of runoff change. Nutrients will be washed from a watershed that can severely affect agriculture production. Water availability is significantly affected, especially in the tropic regions (Gunathilake et al., 2020). These challenges are especially significant in the South Asia region and Sri Lanka, where climate change impact is more pronounced and communities are highly vulnerable (Dissanayaka & Rajapakse, 2019).

The long-term analysis of temperature indicates increasing trend over Sri Lanka. In contrast, average annual rainfall is reported to have a decreasing trend (Wijesekera, 2010). The same study also quoted on Sri Lankan Centre for Climate Change Studies for the National level modelling and stated the temperature decreases during the South-West Monsoon season are anticipated to be 2.5 ℃ whereas the North-East monsoon season have a temperature increase of 2.9 ℃. The significant high changes in rainfall were found for South-West Monsoon than the North-East Monsoon. Such temperature and rainfall changes pose significant challenges on planning water resources and the performance associated with structure for the efficient water resources management in the country.

In Sri Lanka, only a limited number of studies have been undertaken to assess variation of streamflow due to climate change impact. Dissanayake and Rajapakse (2019) evaluated the variation of streamflow in the Kelani River Basin of Sri Lanka under CMIP5 projections of one GCM. On the other hand, in this study, streamflow variation in the KRB is evaluated under CMIP6 projections using multiple GCM output and their ensemble. IPCC recommends the ensemble of multiple climate models since it captures the uncertainty and provides more reliable projections than a single model (Stocker et al., 2010).

There are many hydrological models to simulate rainfall-runoff processes such as Soil and Water Assessment Tool (SWAT), Hydrologic Engineering Centre-Hydrologic Modelling System (HEC-HMS), Variable Infiltration Capacity Model, the HBV-light model, and the J2000 model (Gunathilake et al., 2021). These models are frequently used by hydrological modellers around the world to understand catchment response under different management practices. Application of these numerical models for assessing climate change-related impacts have received significant attention in Sri

Lanka and worldwide. In particular, the HEC-HMS model is extensively used to simulate streamflow, especially for climate change impact studies, and proved to have reasonable accuracy in a long-period simulation run (Dissanayaka & Rajapakse, 2019; Gunathilake et al., 2020; Mahmood et al., 2016). Therefore, HEC-HMS was selected to simulate river flow of KRB.

In this research, future variations of the KRB's streamflow is evaluated under SSPs 2-4.5 and 5-8.5 using the output of three GCMs from CMIP6 – CNRM-CM6-1, MRI-ESM2-0, MPI-ESM1-2-LR, and their ensemble. Change in streamflow is analyzed over different timescales (i.e., daily, monthly, seasonal, and annual). A calibrated and validated Hydrologic Engineering Center – Hydrologic Modelling System (HEC-HMS) was used to model the future streamflow. Further, bias correction is necessary before using direct output from GCMs for climate change impact assessment at watershed/local scale(Fang et al., 2015; Gunathilake et al., 2020; Gutmann et al., 2012; Teutschbein & Seibert, 2012). Therefore, a statistical bias correction procedure was applied to remove bias in daily rainfall, minimum and maximum temperature. Rainfall is bias corrected by the linear scaling method, and temperature is bias corrected by the Variance Scaling method. These bias correction methods were selected as they provided satisfactory results (Fang et al., 2015).

1.2 Problem Statement

Kelani River Basin, situated in the wet zone of Sri Lanka, experiences intense rainfall during monsoon seasons leading to frequent floods. Subsequently, these floods endanger the lives and properties of downstream floodplains in the Kelani River Basin (De Silva & SB, 2015). Moreover, the occurrence and intensity of extreme rainfall are further exacerbated due to climate change impacts that threaten the basin with even more devastating floods. Given the significance of the problem, this study was conducted to understand the behaviour of future floods, droughts, and overall water balance under changing climate, which will contribute to sustainable practices and preventive measures in the context of water resources management.

1.3 Objectives

1.3.1 Main Objective

The main objective of this research is to evaluate the future streamflow variability in the Kelani River Basin using three CMIP6 models, and a combination of their ensemble under SSP 2-4.5 and 5-8.5 scenarios. Change in streamflow is quantified over the near-future (2030-2059) and far-future (2070-2099) concerning the baseline period (1985-2014).

1.3.2 Specific Objectives

1) To set up, calibrate, and validate a suitable hydrologic model (i.e., HEC-HMS) that can project the streamflow of the Kelani River Basin
2) To undertake a thorough bias-correction of raw CMIP6-GCM projected precipitation and temperature data over the Kelani River Basin using suitable statistical approaches
3) To project the future streamflow of the Kelani River over near future and far future periods and quantify change (concerning the baseline period) at different time scales (e.g., daily, seasonal, monthly, and annual)
4) To provide recommendations for river basin planners and managers for sustainable management of water resources of the Kelani River Basin over the 21st century.

CHAPTER 2

2 LITERATURE REVIEW

This chapter presents literature support for the research methodology to be followed in the successive chapter. Specifically, this chapter explains the sixth phase of the global climate model (CMIP6), bias correction of climate data, and hydrologic modelling using the HEC-HMS model.

2.1 Global Climate Model – CMIP6

Coupled Model Intercomparison Project (CMIP) is a project of the World Climate Research Program (WCRP)'s Working Group of Coupled Modelling (WGCM). CMIP's central goal is to advance scientific understanding of the Earth system, leading to increased process understanding in areas including clouds, aerosols, internal variability, the impact of volcanic eruptions on climate, and geoengineering. Since its inception in 1995, CMIP has coordinated climate model experiments involving multiple international modelling teams worldwide. CMIP, with its continuous improvement, has led to a better understanding of past, present, and future climate change and variability in a multi-model framework. CMIP has developed in several phases. The well-known phases start from the third, fifth, and now sixth – CMIP3, CMIP5, and CMIP6, respectively. The Earth System Grid Federation (ESGF https://esgf-data.dkrz.de/projects/esgf-dkrz/) facilitates access and archival to CMIP models output in the standardized formats (Eyring et al., 2016).

The scientific backdrop of CMIP6 experimental design is the Grand Science Challenges (GCs). These GCs from the WCRP strategy accelerate progress in climate science. GCs are related to (1) advancing understanding of the role of clouds in the general atmospheric circulation and climate sensitivity, (2) assessing the response of the cryosphere to a warming climate and its global consequences, (3) understanding the factors that control water availability over land, (4) assessing climate extremes, what controls them, how they have changed in the past and how they might change in the future, (5) understanding and predicting regional sea-level change and its coastal impacts, (6) improving near-term climate predictions, and (7) determining how biogeochemical cycles and feedback control greenhouse gas concentrations and climate change (Eyring et al., 2016).

CMIP6 projections are different from those of CMIP5 and CMIP3 in several ways; first, they use a new version of climate models and projections that combine the new SSPs produced by Integrated Assessment Model (IAM). Second, climate model projections are part of CMIP6-endorsed MIP (Model Intercomparison Project), unlike CMIP5 and CMIP3, where projections are the core experiments. Third, CMIP6 projections start from 2015, whereas CMIP5 projections start from 2006. More new models with high resolution and complexity are added in the CMIP6 (Eyring et al., 2016).

2.1.1 Climate Change Scenarios – Shared Socioeconomic Pathways (SSPs)

Climate change scenarios are developed to evaluate the impact of anthropogenic activities (e.g., greenhouse gases, chemically reactive gases, aerosols, and land use) on the climate system. They play a crucial role in understanding climate-change impacts on society and ecosystems and the effectiveness of response options such as adaptation and mitigation under a wide range of future outcomes (O'Neill et al., 2016). Scenarios originated from the Intergovernmental Panel on Climate Change (IPCC) Special Report on Emissions Scenarios in the third phase of Coupled Model Intercomparison Project (CMIP3) (Nakicenovic et al., 1990). Successively, new scenarios using four pathways of land use, emissions of air pollutants, and greenhouse gases that are known as Representative Concentration Pathways (RCPs) formed projections of the fifth phase of Coupled Model Intercomparison Project (CMIP5) (Stocker et al., 2013).

CMIP6 scenarios (ScenarioMIP) are based on a new set of emissions and land use scenarios produced with integrated assessment models (IAMs) that use future pathways of societal development. The Shared Socioeconomic Pathways (SSPs) combined with RCPs from CMIP5. ScenarioMIP is developed through integrating climate researchers within the climate science (IAM) and impacts, adaptation, and vulnerability (IAV) communities. Under this collaborative approach, it is aimed to enable integrated analysis combining climate models and societal futures. In summary, the ScenarioMIP projects the future either in the presence or absence of climate policies (O'Neill et al., 2016). In case of the absence of climate policies, scenarios are developed without considering climate mitigations on the baseline scenario. However, when climate policies are present, the impact of mitigations measures are considered on the baseline scenario.

SSPs 1and 5 predict an optimistic future based on enormous investments in education and health, rapid economic growth, and well-functioning institutions. SSP1 assumes sustainable development. However, SSP5 assumes fossil-intensive development and shift toward none-sustainable practices. SSPs 3 and 4, with little investment in education or health, a fast-growing population, and increasing inequalities envision a pessimistic future. Countries prioritize regional security in SSP3. On the other hand, SSP4 is driven by significant inequalities between countries, leading to societies vulnerable to climate change impact. SSP2 projections follow historical without having significantly deviating from the historical pattern (O'Neill et al., 2016).

CMIP6 scenarios are based on the parallel approach. As illustrated in Figure 2-1, scenarios vary according to the level of forcing (RCPs) used in the model on one track. The other track depends on alternative future societal development pathways (i.e., the SSPs) generated with IAMs. The ScenarioMIP structure is divided into tier 1 and tier 2. Tier 1 encompasses a wide range of uncertainty in future forcing and developed new SSP scenarios as continuations of the RCP2.6, RCP4.5, and RCP8.5 forcing levels. Moreover, with exceptionally high aerosol emissions and land-use change, an additional unmitigated forcing scenario (SSP3-7.0) developed in this tier. Tier 2 developed four new RCP forcing levels. It includes RCP6.0 and two mitigation scenarios (SSP4-3.4), SSP with forcing level less than RCP2.6 and overshoot pathway (SSP5-3.4-OS) (O'Neill et al., 2016).

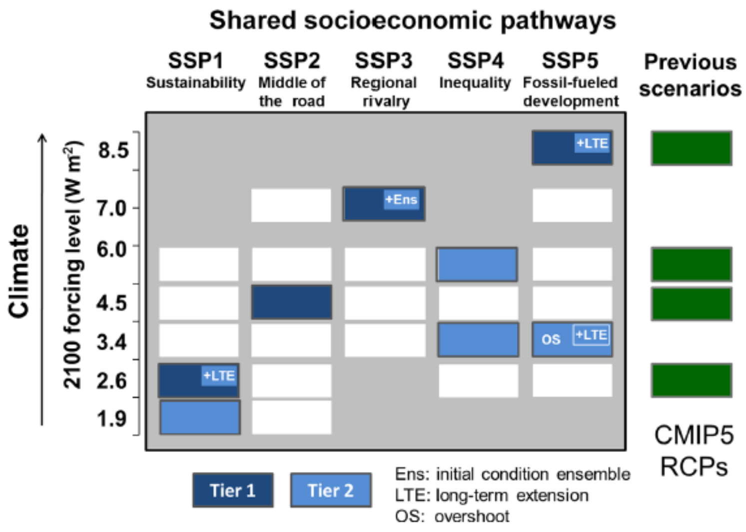

Figure 2-1: Parallel Matrix of CMIP6 scenarios

Source: (O'Neill et al., 2016)

2.1.2 Selected GCMs for This Study

In this study three GCMs (CNRM-CM6-1, MRI-ESM2.0 and EC-Earth3-CC) are selected. CNRM-CM6-1 model is developed for the sixth phase of the Coupled Model Intercomparison Project 6 (CMIP6), sixth generation of fully coupled atmosphere-ocean general circulation model developed by Centre National de Recherches Météorologiques (CNRM) and Centre Europeen de Recherche et de Formation Avancee en Calcul Scientifique (CERFAC), Toulouse 31057, France. The model is an updated version of its predecessor CNRM-CM5.1, developed for the fifth phase of the Coupled Model Intercomparison Project 5 (CMIP5). CNRM-CM6-1 has significant improvements in representing atmospheric and land processes. It has significant reduction of ocean biases in temperature and salinity, improved land surface hydrology representation, including snow (Voldoire et al., 2019).

MRI-ESM2.0 model, developed by Meteorological Research Institute of Japan for CMIP6, is an improved version of MRI-CGCM3 and MRI-ESM1 which participated in the CMIP5. MRI-ESM2.0 has enhanced atmospheric vertical resolution of 80 layers in contrast to MRI-CGCM3 of 40 layers. The new model improvement for clouds has led to noticeable reduction in errors in shortwave, longwave, and net radiation at the top of the atmosphere. The resulting improvement in radiation distribution reduced surface air temperature bias (Yukimoto et al., 2019).

EC-Earth3-CC, along many other EC-Earth3 models, has been developed collaboratively by the European research consortium EC-Earth to provide an integrated tool for Earth system studies for European research community. The model configuration has a description of the carbon cycle, which is used for the Coupled Climate–Carbon Cycle Model Intercomparison Project (C4MIP). Unlike ScenarioMIP where prescribed concentrations are simulated, EC-Earth3-CC allows 360 simulations with emissions forcing. The former EC-Earth2, which was simulated under CMIP5, integrates weather forecasting models from Integrated Forecasting System of the European Centre for Medium-Range Weather Forecasts (ECMWF) and climate change studies into a joint system to predict future. Its updated version, EC-Earth3, incorporates improved physical and dynamic features. These features include new Earth System Model (ESM) components, a flexible system framework, community tools, and improved indicators (Döscher et al., 2021). Interested readers can refer to CMIP6 documentation portal for comprehensive details on the individual models and CMIP6 data in general (https://pcmdi.llnl.gov/CMIP6/).

2.2 Bias Correction of Climate Data

Bias correction is widely used to improve the coarse resolution of GCM/RCM for climate change impact assessment at a watershed scale (Gutmann et al., 2012). Different bias correction methods are developed for removing biases in precipitation and temperature time series from climate models (Teutschbein & Seibert, 2012). Well-known bias correction methods are linear scaling (LS), local intensity scaling (LOCI), Power transformation (PT), distribution mapping (DM) and quantile mapping (QM) in case of precipitation, and linear scaling (LS), variance scaling (VARI) and distribution mapping (DM) for temperature (Fang et al., 2015).

Bias correction methods are categorized as simple linear/nonlinear scaling and sophisticated distribution mapping. The scaling approach corrects the mean or variance of climatic variables through either a linear or nonlinear approach. For instance, linear scaling corrects the mean of desired climatic variable linearly, while power transformation corrects the mean and variance in a nonlinear approach. On the other hand, distribution mapping changes the distribution of raw GCM output to that of observed data (Luo et al., 2018).

The linear scaling method changes the mean of GCM output and makes it equal to the mean of observed time series through the monthly scaling factor (Fang et al., 2015; Luo et al., 2018). The local Intensity Scaling (LOCI) method is used to correct precipitation, and it corrects wet-day frequencies of raw GCM data. Drizzle days, days with little precipitation, can be corrected with this method (Schmidli et al., 2006). Power transformation corrects both mean and variance of precipitation data using a nonlinear approach in an exponential form. Therefore, this method can be more accurate (Fang et al., 2015). Since this method cannot correct wed-day frequencies, precipitation needs to be corrected by the LOCI method first.

Since temperature is a normally distributed variable, the variance scaling method was developed to correct the mean and variance of temperature data (Terink et al., 2010). Distribution mapping (DM) of precipitation/temperature change the distribution of raw data to that of observed ones by changing statics, including mean, standard deviation, and quantiles of raw data (Fang et al., 2015). The method assumes that climatic variables of interest follow a specific distribution (Luo et al., 2018). Quantile mapping of precipitation is an effective method that can be applied to any precipitation distribution. It is an effective approach, capable of correcting the mean, variance, wet-day frequency, and quantiles of precipitation. Selecting a particular approach for bias correction is essential to provide reliable input data for impact assessment at a local/watershed scale (Luo et al., 2018).

From these methods, linear scaling and variance scaling methods are selected to correct bias in precipitation and temperature time series, respectively. The linear scaling method performed well in correcting medium precipitation range, subsequently, a good correlation coefficient was found with this method (Fang et al., 2015). Since this study focuses on overall water balance assessment instead of extremes, this method is selected as it performs well in correcting medium range of precipitation. The variance scaling for temperature was adapted as it corrects both mean and variance of data, and it is recommend for a normally distributed data such as temperature (Fang et al., 2015).

2.3 Hydrologic Models

Hydrologic models are important tools in managing water resources in an integrated and sustainable manner with growing climate change challenges. Broadly, these models are classified into two groups; physical and abstract models (Chow et al., 1988). Physics-based models based on mathematical principles are simplified representations of reality. Physical models can be further classified into scale and analogue. A scale model represents a real system through maintaining relationships between essential aspects of the system. Analogue models use the analogy approach to represent hydrologic components (M. K. Samady, 2017).

Abstract (mathematical) models utilize logical programming languages and mathematical concepts to explain the land phase of the hydrological cycle in space and time. It is categorized as deterministic and stochastic models (Chow et al., 1988). In a deterministic model, known relationships among states and events, while without considering randomness, are used to determine the outcome. A deterministic model for single input values will produce one set of output. However, in the case of the stochastic model, output values can be obtained for a single value of inputs with randomness. A deterministic model can be lumped, distributed, or semi-distributed models (Cunderlik, 2003). In a lumped model, variables are averaged over the entire basin without considering spatial variability. On the other hand, a distributed model accounts for the local variation of parameters across the space or watershed (Beven, 2001).

The application of a fully distributed model has its limitation due to the large number of input data required. As a result, a complete understanding of hydrological basins cannot be achieved without meeting the required data for a distributed model (Samady, 2017). However, a lumped requires fewer input data and it does not account for spatial variation of hydrologic processes (Ghaffari, 2011). The other modelling approach that incorporates both fully distributed and lumped is known as the semi-distributed model. This type has its advantage because it requires fewer input data than a fully distributed model. Moreover, it better represents sub-basin parameters or smaller levels than a lumped model (Jajarmizadeh et al., 2012). This model category is further classified into event-based and continuous models. An event-based model only models a single hydrologic event such as storm, flood, soil moisture, for a relatively short period. In contrast, continuous hydrological models simulate multiple state variables (e.g., soil moisture, surface storage) for a more extended period (Samady, 2017).

A wide range of modelling software is developed for continuous hydrologic modelling such as SWAT, HEC-HMS, WEAP, etc. SWAT is a semi-distributed and comprehensive model widely applied to evaluate management practices and climate change impact on the hydrologic cycle at the watershed scale (Arnold & Fohrer, 2005; Fang et al., 2015; Setegn et al., 2011). Many others have used the HEC-HMS model to study climate change impact on streamflow (Dissanayaka & Rajapakse, 2019; Gunathilake et al., 2020; Mahmood et al., 2016).

2.4 HEC-HMS model

Hydrologic Engineering Center – Hydrologic Modeling System (HEC-HMS) is a widely applied software to model runoff from a dendritic watershed system with the given input precipitation data. The model's merits lie in its free availability and relatively easy-to-use interface. It can be applied in small-scale and large-scale watersheds, and a larger watershed can be developed by dividing it into sub-basins. It can model a watershed in a lumped, semi-distributed, or fully distributed manner (USACE, 2016). The model has three main components: basin model, the meteorological model, and control specifications (Alazzy et al., 2017), where the model user can specify desired methods and boundary conditions for the simulation.

HEC-HMS model has been used for flood forecasting, post-fire response analysis, stormwater management, and climate impact assessment. It can run both continuous and event-based simulations. Continuous modelling differs from event-based modelling as it accounts for evapotranspiration, infiltration, percolation, and other losses (Gebre, 2015; Nasimi, 2018; Samady, 2017). Evapotranspiration in HEC-HMS can be modelled using either deficit and constant or soil moisture accounting (SMA) loss method. The deficit and constant loss method use a single layer to account for the change in moisture content. The canopy method, which is required for this method, extracts water from the soil in response to evapotranspiration. The canopy will extract more water from the soil during the dry period between two precipitation events. As a result, the soil layer will dry out. Percolation to deep ground layers only occurs after soil becomes saturated (USACE, 2016).

Soil Moisture Accounting (SMA) method simulates runoff over time in five different layers of storage (HMS, 2000). The five storage layers are canopy interception, surface depression storage, soil, upper groundwater, and lower groundwater (Sampath et al., 2015). For simulation hydrologic processes in these five layers, 12 parameters need to be estimated. Several parameters need to be determined to simulate the movement of water in different storage zones. These parameters include the maximum depths of each storage zone, the percentage that each storage zone is filled at the beginning of the simulation, and the transfer rates, such as the maximum infiltration rate (Nasimi, 2018).

The schematic in Figure 2-2 shows a conceptual representation of the SMA method. Precipitation is used as input in the SMA model and routed through the canopy, surface, and soil storages. Groundwater and evapotranspiration are considered at different stages before the generating the final streamflow hydrograph (Nasimi, 2018).

Canopy and surface storage must be filled before infiltration/surface runoff within the SMA loss model. After the two storages are filled, the water will either infiltrate or become a direct surface runoff. The infiltrated water first fills the tension zone, followed by the upper zone. After the upper zone is filled, precipitation can percolate from the upper zone into the groundwater layer 1 (GW1) storage. However, water cannot enter from the tension zone. Some water in GW1 is routed to the first base flow reservoir while the rest percolates to groundwater layer 2 (GW2). From GW2, water can be transferred to the second base flow reservoir.

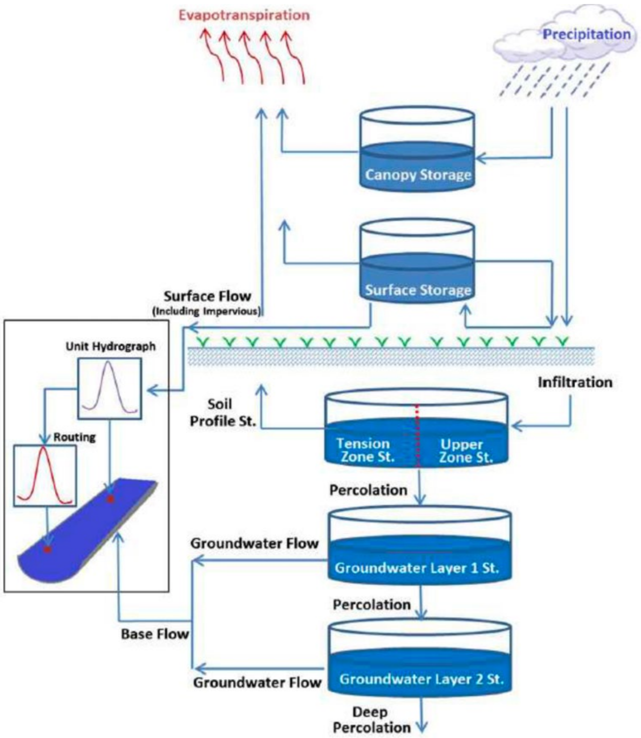

Figure 2-2 Conceptual Representation of Soil Moisture Accounting

Source: (Nasimi, 2018)

In this study, HEC-HMS with the SMA method is selected for continuous hydrologic modeling and climate change impact assessment because the method provides acceptable results for continuous simulation (Dissanayaka & Rajapakse, 2019; Nasimi, 2018). Many other authors successfully applied HEC-HMS with this loss method for climate change impact assessment (Dissanayaka & Rajapakse, 2019; Gunathilake et al., 2020).

2.5 Previous Studies Assessed Climate Change Impact on Streamflow

Gunathilake et al. (2020) evaluated projected streamflow from three RCMs of CORDEX in the Nan River Basin, Thailand, under RCP 4.5 and 8.5. Results from the temperature trend revealed increasing temperature in future projection compared to the baseline period, with more temperature increase in the latter part of the 20th century. Precipitation decreased under future projection, especially during the wet period. As a result, decreasing streamflow was obtained under both RCPs considered. While examining the flow duration curve for different time windows, a decrease in high flows and an increase in low flows were found for the projected periods in 2020–2039 (2030s), 2040–2069 (2050s), and 2070–2099 concerning the base period (1988–2005).

Givati et al. (2019) applied an ensemble of 19 regional climate models to assess water availability of the upper Jordan River in Israel under RCP 4.5 and 8.5 scenarios. Their results indicate that projected precipitation in the future may decreased under RCP 4.5 and 8.5, respectively compared to the baseline period (1979-2005). In addition, far-future precipitation (2050-2079) decreased more than in the near-future (2020-2049). The decrease in precipitation was attributed to the increase in evapotranspiration. Accordingly, the modelled streamflow for different projections showed decreased streamflow. A nonlinear decrease of streamflow compared to precipitation was also projected in this study.

Mahmood et al. (2016) investigated climate change impact on streamflow in the Kunhar River basin, Pakistan using HEC-HMS hydrologic model. Here, change in streamflow was evaluated for future periods (2011–2040, 2041–2070, and 2071–2099) concerning the baseline period (1961–1990) under the A2 and B2 scenarios of the HadCM3 global climate model. The results indicate an overall increase in mean annual flow under both A2 and B2 scenarios. The seasonal analysis of streamflow suggested a noticeable increase in summer and autumn and a decrease in spring and winter seasons.

Evaluation of flow duration curve revealed an increase in high and medium flow, while low flow showed decreasing trends for all the project periods and scenarios. The increase in high flow was attributed to increased precipitation in the monsoon season and an increase in medium flow as associated with increasing average annual precipitation. This implies that the basin will experience increasing floods and droughts in the future (Mahmood et al., 2016).

CHAPTER 3

3 MATERIALS AND METHODS

This chapter presents the details of the study area, input data used in the research, general methodology applied in the research, bias correction of climate data, model development, model calibration, and validation. A significant portion of this chapter revolves around hydrologic model development, calibration, and validation.

3.1 Study Area

The Kelani River Basin has the second largest river in Sri Lanka, the Kelani River. The basin is located between Northern latitudes 6.780 – 7.080 and Eastern longitudes 79.870 – 80.220 with a total drainage area of 2,230 km^2. The basin is located in the country's wet zone and intermediate zone according to National Clearing House Mechanism. Situated in hydrologic zone III, basin receives an average annual rainfall of 2,400 mm (De Silva & SB, 2015). The upper part of the basin is characterized by mountainous terrain, less urbanized, and covered with vegetation. The lower part is characterized by flat terrain and highly urbanized areas. During monsoons, the river discharges approximately 800-1500 m^3/s into the Indian Ocean. Since Sri Lanka is located tropical region, the weather condition in the Kelani basin and the whole country is dominated by two distinct monsoon seasons – Northeast (December-March) and Southwest (May-September). Downstream of the basin experiences intense floods during Southwest Monsoon, which frequently triggers substantial damages to the society and economy (De Silva & SB, 2015). In this study, the basin's upstream catchment from Hanwella hydrometric station, known as Hanwella watershed, is considered for analysis (Figure 3-1). The Theisen map with the corresponding rain gauges and the number of sub-basins considered are presented in Figure 3-2.

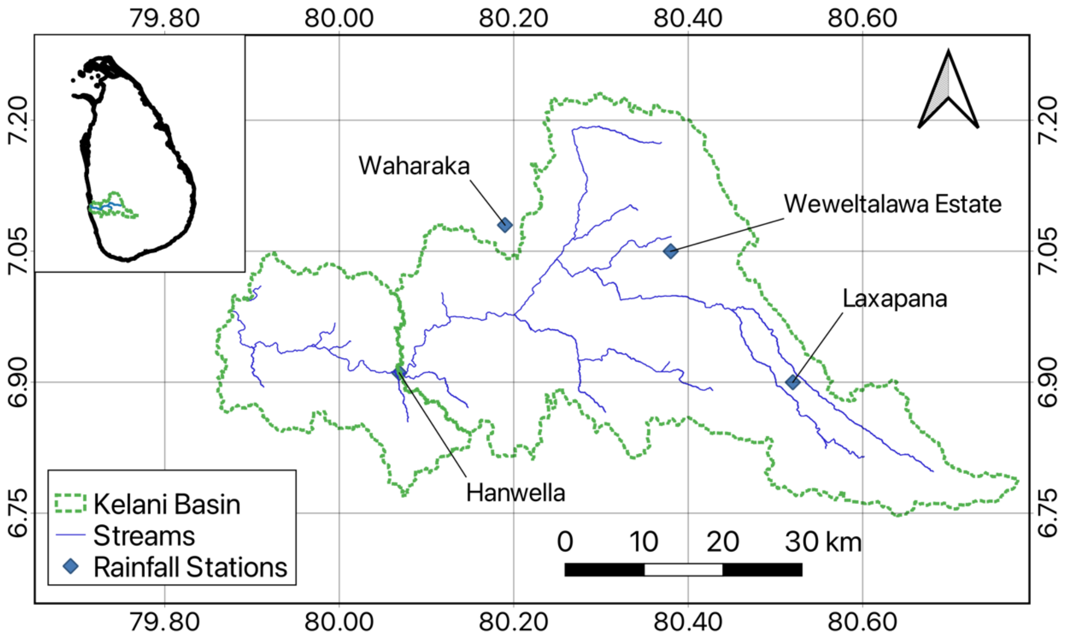

Figure 3-1: Study Area - Kelani Basin

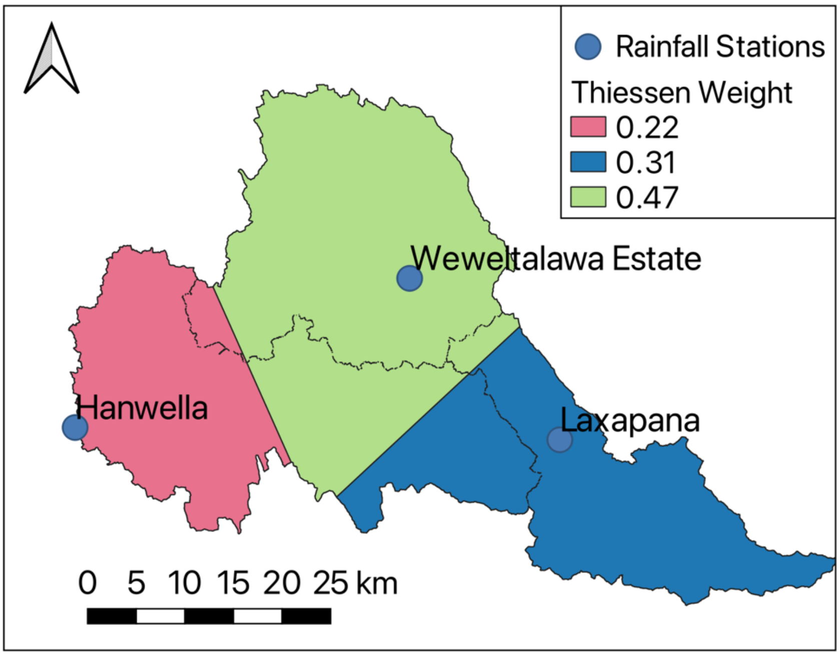

Figure 3-2: Thiessen Rainfall Map of Hanwella Watershed

3.2 Data Collection

Data required for this study are collected from different sources. Observed hydrometric data (No 1 to 5) in Table 3-1 are collected between the years 1985 – 2014 from designated sources. These data types are required for bias correction of climate data and calibration/validation of the hydrologic model. In addition, Table 3-2 provides the geographic coordinate of each gauging station for the corresponding data type. Geospatial data, including Digital Elevation Model (DEM), was collected for watershed delineation. Further, Esri 2020 Land Cover was obtained from the Impact Observatory website. The new land cover is developed from the Sentinel-2 mission at 10 m resolution. Moreover, each model's climate data (Table 3-3) was downloaded from Copernicus Climate Data Store (CDS).

Table 3-1: Observed Hydroclimatic and Geospatial Data

No	Data Type	Extent	Resolution	Source
1	Rainfall	Hanwella	Daily	Meteorological Department
		Laxapana	Daily	
		Waharaka	Daily	
		Weweltalawa	Daily	
2	Streamflow	Hanwella	Daily	Irrigation Department
		Kithulgala	Daily	
		Wellawaya	Daily	
3	Minimum Temperature	Colombo	Daily	Meteorological Department
4	Maximum Temperature	Colombo	Daily	Meteorological Department
5	Evapotranspiration	Colombo	Daily	Meteorological Department
6	DEM	Kelani Basin	30 m	Survey Department
7	Esri 2020 Land Cover	Kelani Basin	10 m	Esri Inc.

Table 3-2: Coordinates of all Gauging Stations with Their Corresponding Data Type

Data Type	Station	Coordinates (Degrees)	
		North Latitude	East Longitude
Rainfall	Hanwella	6.91	80.08
	Laxapana	6.9	80.52
	Weweltalawa Estate	7.05	80.38
Streamflow	Hanwella	6.91	80.08
Minimum Temperature	Colombo	6.90	79.87
Maximum Temperature	Colombo	6.90	79.87
Evapotranspiration	Colombo	6.90	79.87

Table 3-3: Meta Data of Climate Models

Model	Nominal Resolution (km)	Spatial Resolution (Degrees)		Variant Label	Institution ID
		East Longitude	North Latitude		
CNRM-CM6-1	250	1.40625	1.400768	r1i1p1f2	CNRM-CERFACS
MRI-ESM2-0	100	1.125	1.12149	r1i1p1f1	MRI
EC-Earth3-CC	100	0.703125	0.701753	r1i1p1f1	EC-Earth-Consortium

3.3 Data Checking

3.3.1 Identification of Missing Records in Daily Data

Input data were systematically examined to determine missing values, if any, before proceeding to the gap-filling of data. All data types and their corresponding stations are examined for missing and other abnormal records. Each time series was evaluated based on standard dates and identified the missing dates. In addition to the missing (blank) records, abnormal records in each time series were also treated as missing records. Abnormal records consist of negative values and typos in data. Table 3-4 summarizes the result of this check and provides details of missing records.

Table 3-4: Summary of Missing Days of Hydrometric Data (1985-2014)

Data Type	Station	Number of Missing Days	Percent of Missing Data
Rainfall	Hanwella	153	1.40
	Laxapana	30	0.27
	Weweltalawa	151	1.38
Streamflow	Hanwella	228	2.08
Minimum Temperature	Colombo	46	0.42
Maximum Temperature	Colombo	0	0.00
Evapotranspiration	Colombo	56	0.51

3.3.2 Gap Filling of Missing Time Series

Missing records were filled by applying different methods for different respective data types. The normal ratio method was applied to fill the gap in each rain gauge station for the rainfall data. The normal ratio method is applicable when the average annual rainfall of neighbouring stations exceeds 10% of the target station to be gap-filled (Sattari et al., 2017). It was determined that the average annual rainfall of the neighbouring stations exceeds 10% of the target station, and hence this method was adopted. Streamflow data were gap-filled using linear interpolation. As data from other stations contained missing records in the same period, other methods of gap filling which rely on neighbouring stations could not be applied. Likewise, gaps in minimum, maximum temperature and evapotranspiration were filled using linear interpolation as the available data was limited to only one station for each of these data types, and the length of missing records was short. Here, interpolation was done using Hydrologic Engineering Centre Data Storage System, HEC-DSS.

3.3.3 Consistency Check for Rainfall Data

Before applying rainfall from a gauge for study, it is necessary to check the precipitation trend to ensure that the trend in rainfall data is due to meteorological factors not to change in gauge location (James & Clayton, 1960). Therefore, rainfall data are checked with single and double mass curve methods to evaluate each rain gauge's consistency and long-term trend relative to each other. Daily rainfall and single mass curve – cumulative daily rainfall for each station – are plotted to visually determine abnormal records and compare commutative precipitation of each gauge (Figure 3-3). It shows high rainfalls of Laxapana station during 1990, which could be due to an extreme event or error in the gauge. The single mass curve reveals consistent behaviour of Hanwella, Laxapana, and Weweltalawa rain gauge stations. Moreover, cumulative daily rainfall shows a higher volume of rainfall at Laxapana, Weweltalawa, and Hanwella, respectively. Likewise, the double mass curve in Figure 3-4 shows a similar consistent trend.

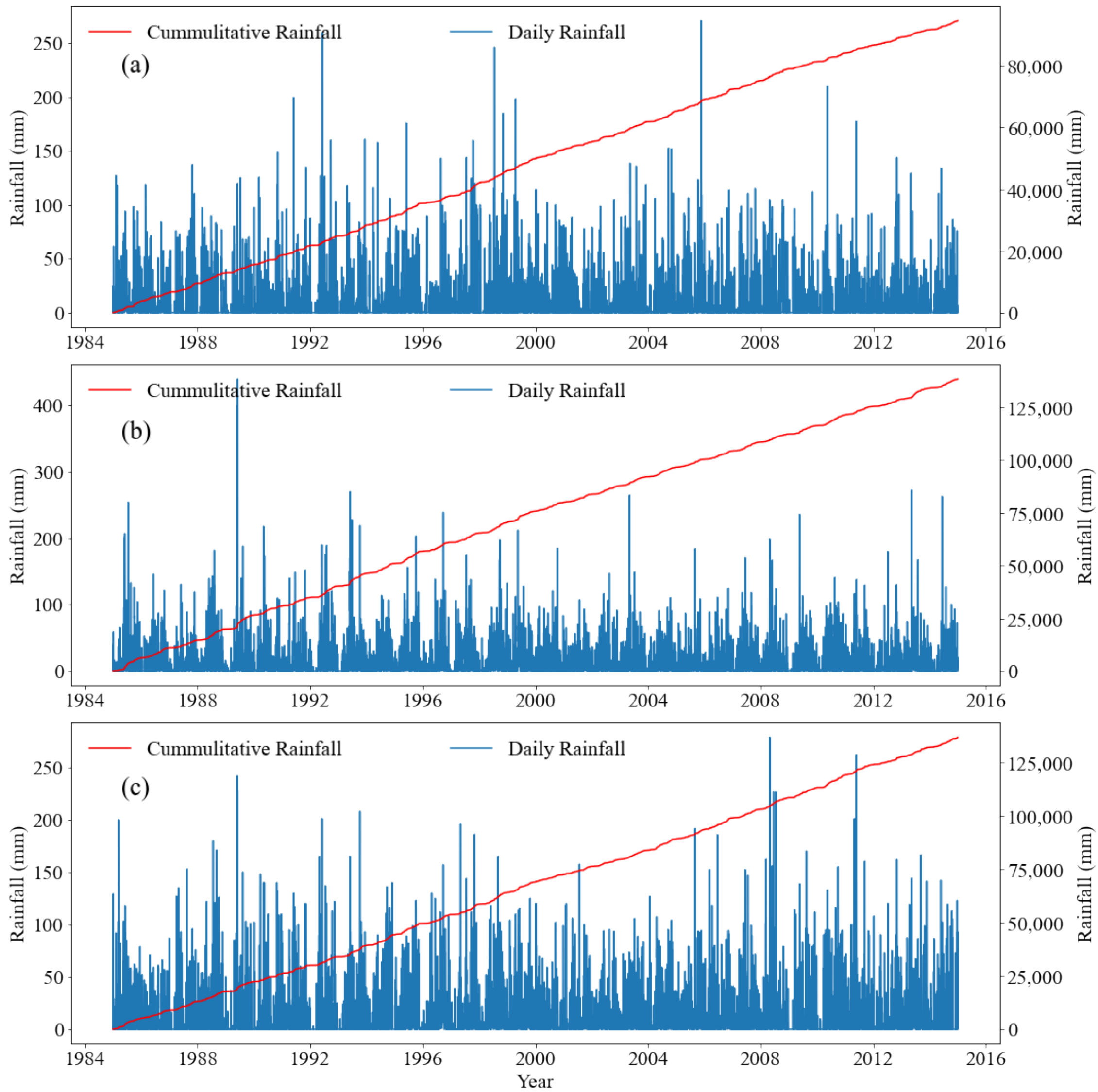

Figure 3-3: Daily and Cumulative Daily Rainfall for Each Rain Gauge - Hanwella (a), Laxapana (b) and Weweltalawa (c) stations

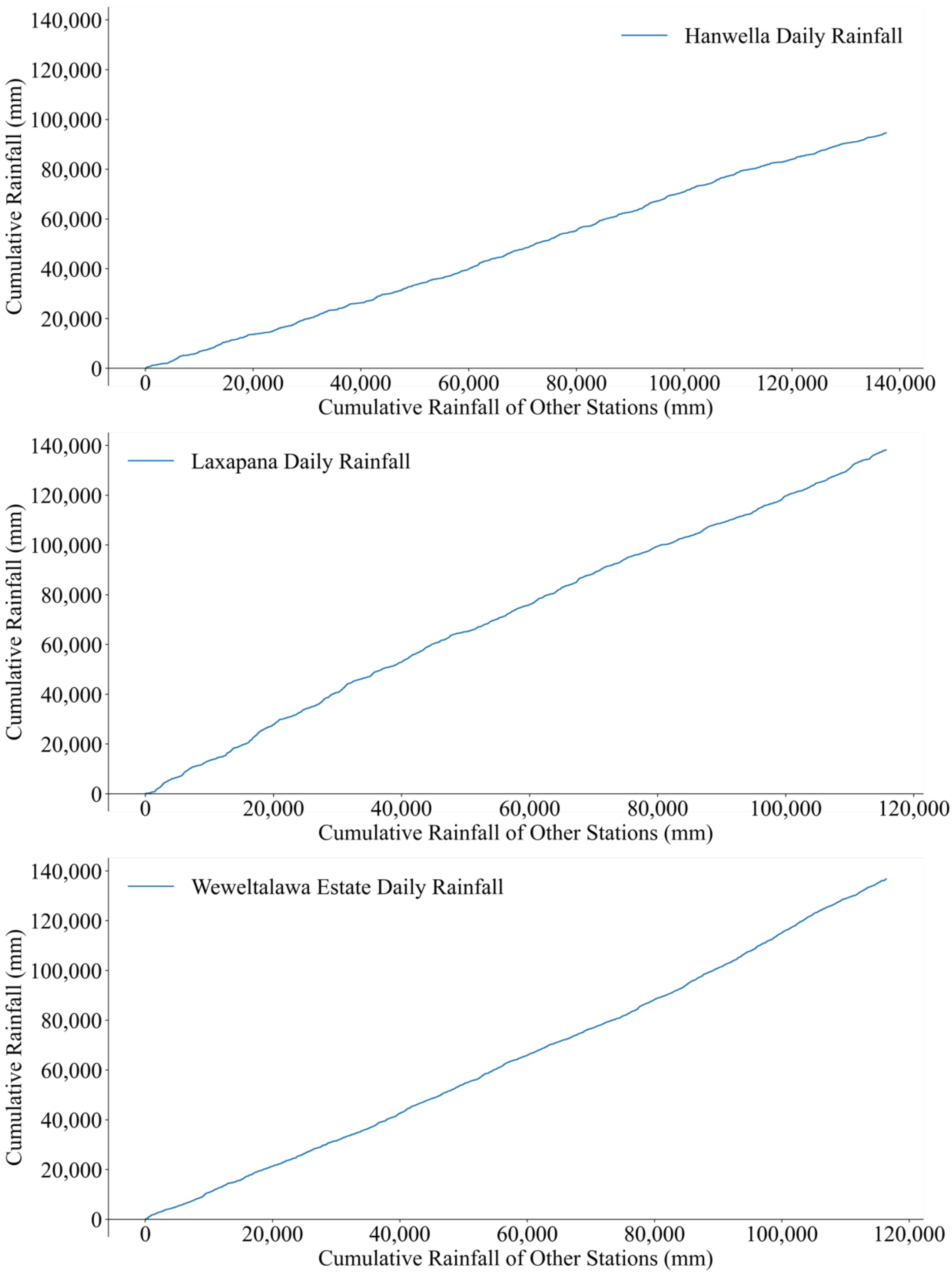

Figure 3-4: Double Mass Curve of Each Rain Gauge

3.3.4 Evaluating Data Trend

3.3.4.1 Daily Time Series

Data are visually examined under different time scales with various plots to determine outliers, the correlation between rainfall and runoff, and other anomalies. The plot of daily streamflow at the Hanwella stream gauge and daily rainfall obtained from the Thiessen weight of each rain gauge (Figure 3-5) suggests an acceptable correlation between streamflow and rainfall. Expectedly, high streamflow occurs after a certain lag time from high rainfall events.

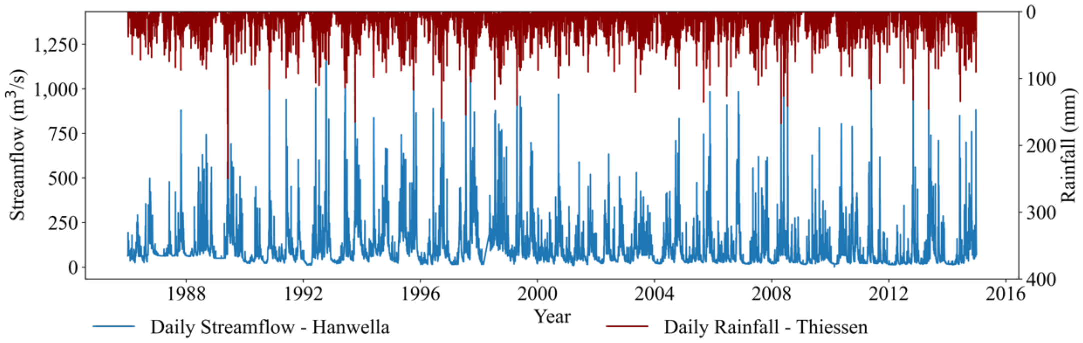

Figure 3-5 Thiessen Rainfall vs. Hanwella Streamflow

3.3.4.2 Monthly Time Series

The monthly rainfall distribution for each rain gauge station is evaluated through the boxplot (Figure 3-6). All gauge stations have a similar seasonal pattern. Comparison of each gauge shows Hanwella has least rainfall distribution variability. In contrast, other stations for most of the months reveal higher variability, which is indicated by 25^{th} and 75^{th} quartiles of boxplots. Additionally, the months of January, February, March, and December can be categorized as having lower rainfall intensity and variation. On the other hand, rainfall intensity and variation are high during May, June, October, and November, and the rest of the months are falling in-between. Overall, Laxapana and Weweltawala have higher rainfall intensity (0-1500 mm) compared to Hanwella station (0-900 mm).

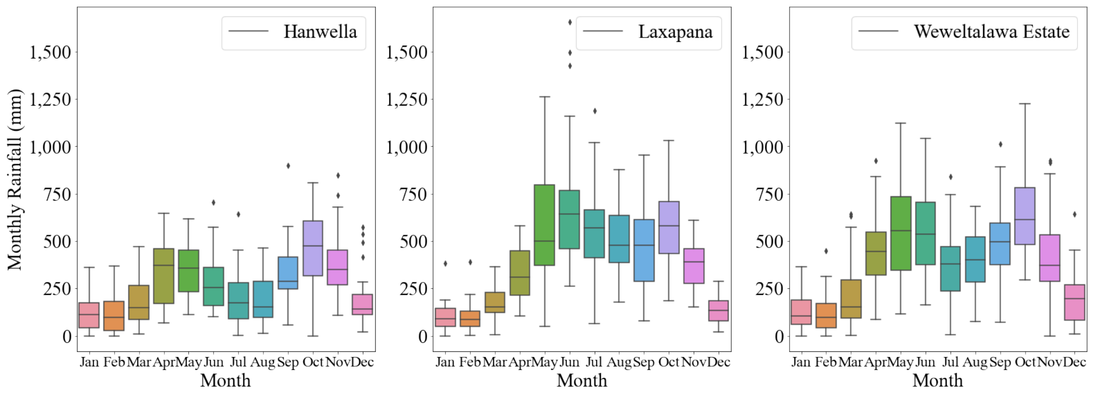

Figure 3-6: Boxplot of Monthly Observed Rainfall for each Gauging Station

3.3.4.3 Annual Time Series

At Hanwella and Laxapana stations, the annual trend (Figure 3-7) shows decreasing precipitation rate over time. However, Weweltalawa reveals increasing precipitation in recent years. The water balance (Figure 3-8) shows that the overall annual streamflow trend follows annual rainfall.

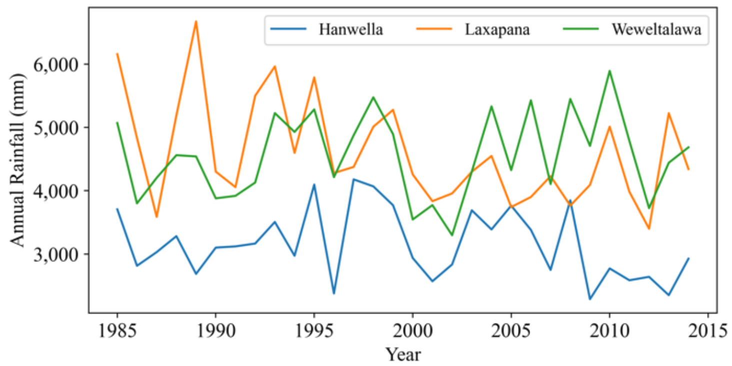

Figure 3-7 Annual Rainfall of Each Rainfall Station

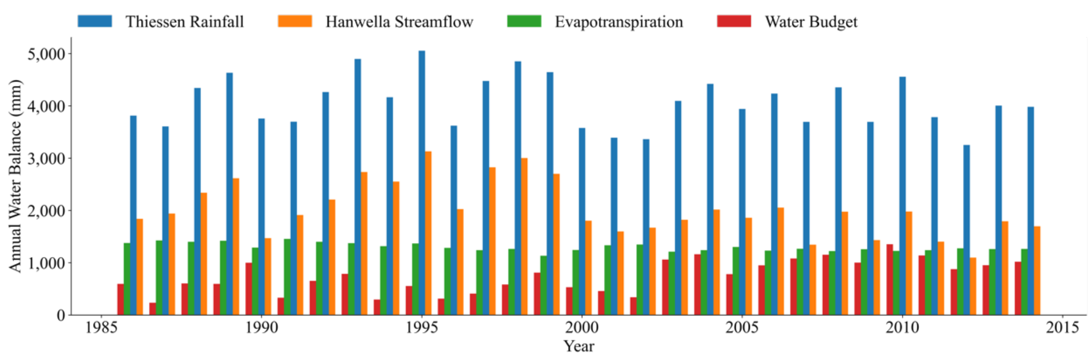

Figure 3-8 Annual Water Balance (Water Budget)

3.4 Methodology

This research evaluates the change in variation of streamflow using output from three CMIP6 models (CNRM-CM6-1, EC-Earth3-CC, MRI-ESM2-0) and their ensemble under SSP 2-4.5 and SSP5-8.5 scenarios. The multiple GCMs modelling approach was applied to capture the uncertainty of projected streamflow with different models and provide more reliable projections with an ensemble model (Stocker et al., 2010). The ensemble of multiple GCM/RCM models was also used by previous researchers to assess projected streamflow under climate change scenarios (Bhatta et al., 2019; Gunathilake et al., 2020; Shrestha, et al., 2016).

Further, the ensemble was obtained by averaging the time series of the three GCM outputs with equal weight for a corresponding rainfall/temperature gauge (Givati et al., 2019; Gunathilake et al., 2020). The time frame for analysis is divided into three separate periods: historical (1985 – 2014), mid-century (2030 – 2059), and late-century (2070 – 2099) periods. The change in streamflow, hydrologic extremes, and overall water balance patterns are examined using various statistical analyses from historical to projected periods under different temporal scales.

Before applying direct output from GCM, downscaling and bias correction of the climate model are necessary to improve the coarse resolution of GCM/RCM for climate change impact assessment at the watershed or local scale (Gunathilake et al., 2020; Gutmann et al., 2012; Teutschbein & Seibert, 2012). Here, bias in precipitation time series is corrected using the linear scaling (LS) method. This method corrects the mean of data and has good performance in improving the correlation coefficient. (Luo et al., 2018; Teutschbein & Seibert, 2012). Daily minimum and maximum temperature are bias-corrected using the Variance Scaling (VARI) approach. VARI method is recommended for bias correction of a normally distributed parameter such as temperature (Fang et al., 2015; Teutschbein & Seibert, 2012).

The hydrologic modelling was performed using the HEC-HMS model. The simple canopy and surface methods were used to account for initial abstraction due to evapotranspiration and surface depressions. Baseflow was modelled with the recession method because other researchers have used it extensively (Nasimi, 2018). Snyder unit hydrograph is applied as a transform method since it provides satisfactory results in an ungauged medium-sized watershed (Chow et al., 1988). The Soil Moisture Accounting (SMA) method is selected for the loss model because other researchers recommend it for continuous hydrologic modelling (HMS, 2000; Nasimi, 2018). The Muskingum method is applied for channel routing since it is widely used with reasonable accuracy for a mild-slope watershed (Song et al., 2011). Evapotranspiration is an essential component that must be modelled in the hydrologic cycle. Therefore, the Hargreaves method was used to model evapotranspiration, which uses the daily minimum and maximum temperature. This method is extensively applied globally especially in the data-scarce watersheds, as it models evapotranspiration with reasonable accuracy and minimal input data (Hargreaves & Allen, 2003). A summary of all these methods/tools used in this research are shown in the methodology flow chart Figure 3-9. Boxes in the left-hand side, as explained before, indicate methods used in HEC-HMS for the respective model component. The initial value of a parameter for the corresponding model component was estimated from available data/literature. These initial values are adjusted during model calibration (1997-2001) to obtain optimized parameters. Further, with the same set of optimized parameters, model was validated for 2002-2006. The observed time series listed in the topmost right corner are used for model calibration/validation and bias-correction of climate data. Bias-corrected GCM data are fed into model to project future streamflow. The changes in streamflow is calculated from historical to the corresponding mid-century and end-century period by averaging discharge time series under annual, monthly, and seasonal time resolutions.

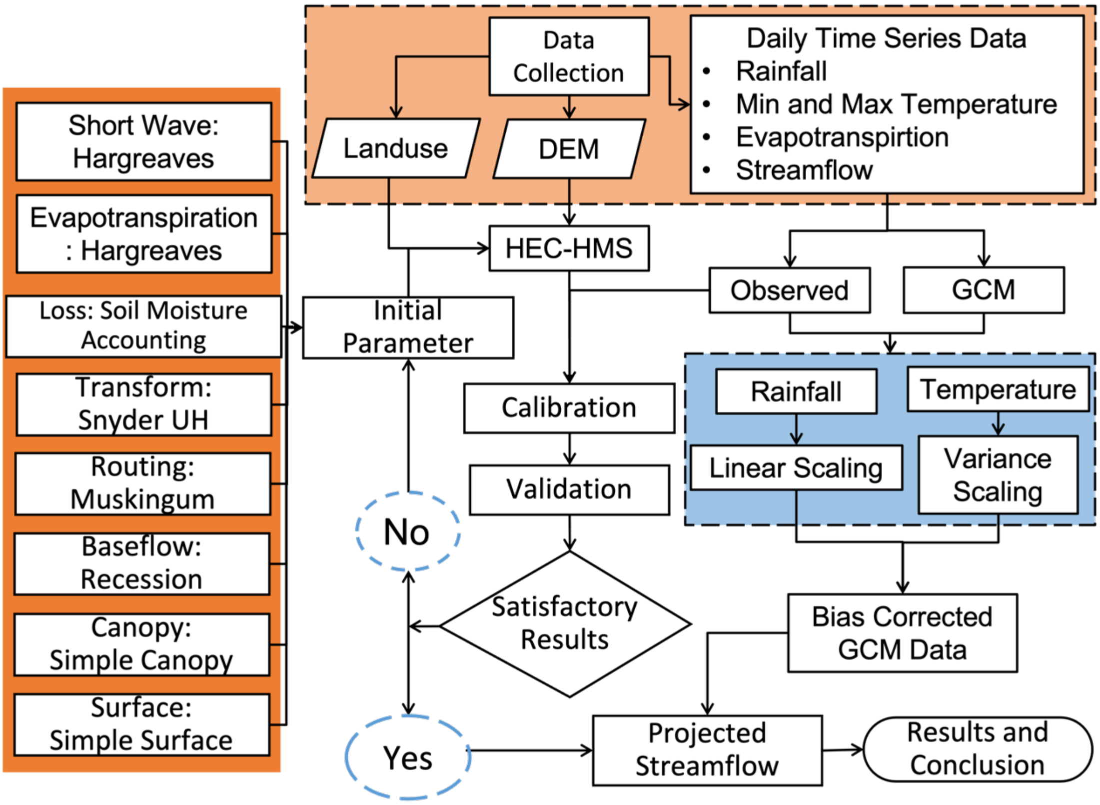

Figure 3-9: Methodology Flow Chart

3.4.1 Bias Correction of Precipitation and Temperature Time Series

This study adapted statistical approaches to eliminate bias in daily GCM precipitation, minimum and maximum temperature. As explained in successive sections, linear scaling and variance scaling methods are used to correct the bias of precipitation and temperature data, respectively. Bias correction of temperature is performed in Climate Model Data for Hydrologic Modeling (CMhyd) tool because it can extract and bias correct climate data (Zhang et al., 2018).

3.4.1.1 Bias Correction of Precipitation – Linear Scaling Method

The linear scaling (LS) method of bias correction is selected to correct the bias of climate data obtained from the global models. This method underestimates high precipitation while overestimating low precipitation. Hence, it may not yield good results in the context of extreme event-related studies (Fang et al., 2015). However, LS performs well in correlation coefficient and correcting overall bias in the data. Since the research is not focusing on extreme analysis, the method is used for bias correction. This method corrects the mean of monthly precipitation; as such. the mean of corrected data should equal that of observed data. LS method corrects precipitation using Equation [3-1].

$$P_{cor,\ m,\ d} = \frac{\mu(P_{obs,\ m})}{\mu(P_{raw,\ m})}\ X\ P_{raw,\ m,\ d} \qquad [3\text{-}1]$$

where μ represents the mean of $P_{obs,\ m,}$ and $P_{raw,\ m}$. $P_{obs,\ m,}$ and $P_{raw,\ m}$ refer to monthly observed precipitation and precipitation of the climate models, respectively. $P_{cor,\ m,\ d}$ and $P_{raw,\ m,\ d}$ represents daily corrected and GCM precipitation, respectively.

3.4.1.2 Bias Correction of Temperature – Variance Scaling Method

Variance Scaling (VARI) can correct both the mean and variance of a normally distributed variable like temperature (Teutschbein & Seibert, 2012). Hence this method was selected to bias correct minimum and maximum daily temperature time series. Corrected daily temperature ($T_{cor,\ m,\ d}$) is obtained using Equation [3-2].

$$T_{cor,\ m,\ d} = [T_{raw,\ m,\ d} - \mu(T_{raw,\ m})]\ \frac{\sigma(T_{obs,\ m})}{\sigma(T_{raw,\ m})} + \mu(T_{obs,\ m}) \qquad [3\text{-}2]$$

where σ and μ represent the standard deviation and mean of $T_{obs,\ m,}$ and $T_{raw,\ m}$. $T_{obs,\ m,}$ and $T_{raw,\ m}$ refer to monthly observed temperature and temperature from the climate models, respectively. $T_{cor,\ m,\ d}$ represents daily corrected temperature, and $T_{raw,\ m,\ d}$ shows daily temperature from the climate model.

3.4.2 HEC-HMS Model

The watershed is modelled with HEC-HMS by dividing it into three sub-basins. Table 3-5 provides a summary of the methods used under each component. Depending on the method used for a particular component, the required parameters varies accordingly. The method of determination designates that how a particular parameter is estimated for the initial modelling. Before proceeding to the calibration of the model, it is important to estimate the initial for a required parameter since it makes the calibration process easier. Additionally, this initial estimation of parameters helps determine a calibrated (optimized) parameter close to the observation. Successive sections provide a detailed explanation of how each of these parameters for the respective component is estimated.

Table 3-5: Summary of the Methods Used and Estimation of Initial Parameters for the Corresponding Method

Component	Method	Required Parameter	Method of Determination
Canopy	Simple Canopy	Initial Storage (%)	Taken from literature
		Maximum Storage (mm)	Derived from land use
Surface	Simple Surface	Initial Storage (%)	Taken from literature
		Maximum Storage (mm)	Derived from terrain and slope
Baseflow	Recession	Initial Discharge (m^3/s)	Taken from literature
		Recession Constant	Taken from literature
		Ratio to Peak	Taken from literature
Transform	SCS Unit Hydrograph	Lag Time (hr)	Estimated from watershed characteristics
		Peaking Coefficient	Taken from literature
Loss Method	Soil Moisture Accounting	All the Parameters in the Appendix (Table 7-1)	All parameters are taken from previous studies in the basin
Routing	Muskingum	K (hr)	Estimated from stream characteristics
		x	Taken from literature
Evapotranspiration	Hargreaves	Hargreaves Coefficient	Taken as default
Short Wave	Hargreaves	Meridian	Obtained from basin coordinate
		Coefficient K	Taken as default

3.4.2.1 Watershed Delineation

The overall model development and watershed demarcation are performed in HEC-HMS 4.9 beta 6. Using a 30 m DEM from Survey Department, the watershed is delineated with the GIS tool in HEC-HMS. A stream threshold of 40 km^2 is used for stream identification. The generated streams and watershed boundary were also validated with the open street map (OSM) of QGIS. The whole watershed is divided into three sub-basins at the Kithulgala, Glencourse, and Hanwella outlets. It is worth mentioning that this sub-basin division was based on terrain characteristics and the availability of streamflow records at the respective locations. Figure 3-10 shows the demarcated sub-watersheds and stream networks.

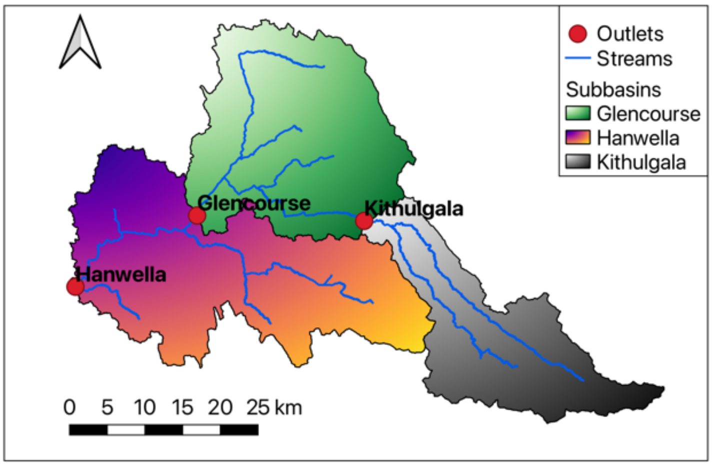

Figure 3-10: Sub-watersheds with Their Respective Outlets and Stream Network

3.4.2.2 Canopy Storage

For continuous modelling, canopy storage is required to account for precipitation loss due to the evapotranspiration of plants. The volume of water captured by plants, trees, and vegetation is quantified in canopy storage within the HEC-HMS model. HEC-HMS has different methods to model canopy storage. Here, the simple canopy method is selected since it has minimal input data requirements. Canopy storage is related to the land use type (Bennett & Peters, 2004). Accordingly, the canopy layer for the watershed is prepared using Esri 2020 Land Cover (Figure 3-12a) and Table 3-6. The resultant canopy layer (Figure 3-11b) is averaged over each sub-basin using zonal statistics in QGIS to obtain respective canopy storage volumes of the corresponding sub-basin.

Table 3-6: Canopy Storage Values for Different Land Use Type

Vegetation type	Canopy interception (mm)
General vegetation	1.27
Grasses and deciduous trees	2.032
Trees and coniferous trees	2.54

Source: (Bennett & Peters, 2004)

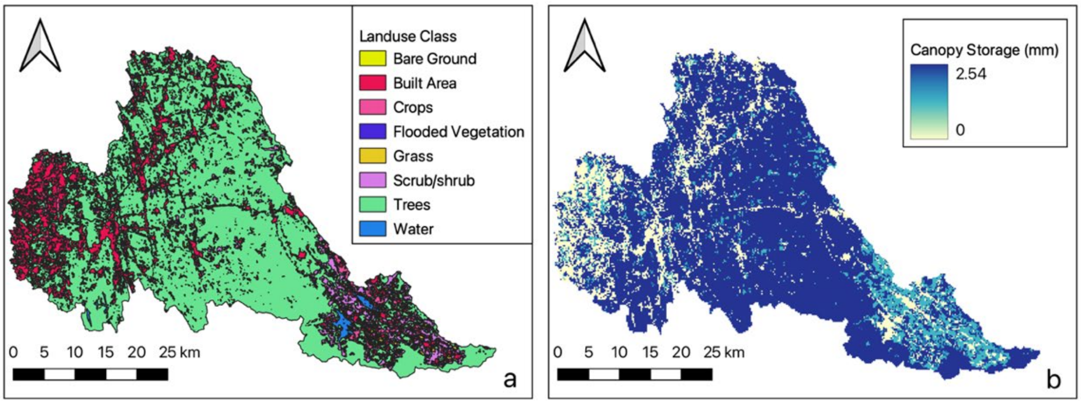

Figure 3-11: Land use Map (a) with Respective Canopy Layer (b) for Watershed

3.4.2.3 Surface Storage

The volume of water stored by surface depressions is known as surface storage. No direct runoff or infiltration occurs until surface depressions are filled. It is dependent on terrain/slope characteristics (Bennett & Peters, 2004). HEC-HMS can model this storage in different methods. A simple surface method, which requires maximum storage to be specified, is selected for this study. A slope map was developed to prepare the surface storage layer (Figure 3-13a). Successively, a surface storage raster layer (Figure 3-13b) was created using reference Table 3-7. The final storage for each sub-basin is obtained by averaging the surface storage layer over each sub-basin (Table 3-8). The final storage of canopy for each sub-basin is also tabulated in the same table.

Table 3-7: Surface Storage Values for Various Slope Classes

Description	Slope %	Surface storage (mm)
Paved impervious areas	NA	3.2 - 6.4
Steep and smooth slopes	>30	1
Moderate to gentle slope	5-30	12.7 - 6.5
Flat and furrowed land	0-5	50.8

Source: (Bennett & Peters, 2004)

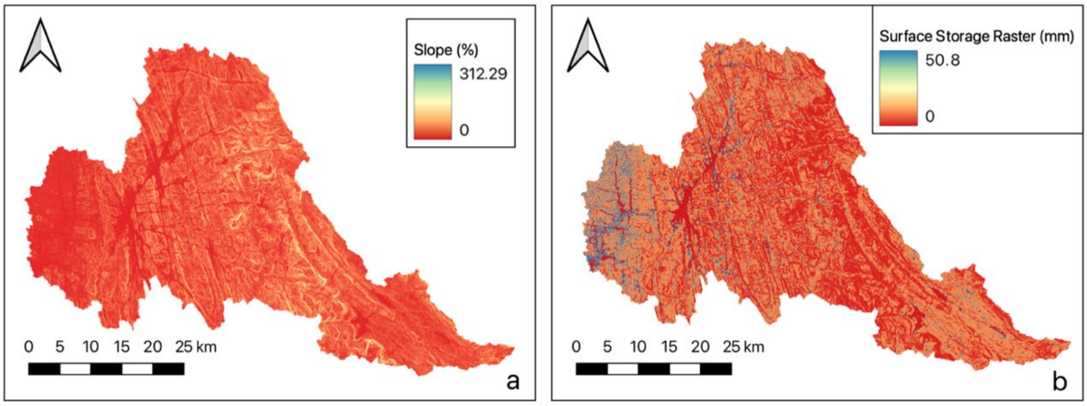

Figure 3-13: Slope Map (a) and Surface Storage Layer (b) for Watershed

Table 3-8: Summary of Canopy and Surface Storage of Sub-basins

Sub-basin	Maximum Canopy Storage (mm)	Maximum Surface Storage (mm)
Kithulgala	1.92	7.27
Glencourse	2.12	7.74
Hanwella	1.95	11.00

3.4.2.4 Baseflow Method

For the baseflow modelling, the recession method is applied. It has been applied in different parts of the world to model baseflow (Nasimi, 2018). This method establishes a direct relationship between the base flow at any time and the initial baseflow using recession constant, as shown in Equation [3-3]. Initial baseflow is a boundary condition and should be taken as an average flow likely to occur at the start of a storm runoff (HMS, 2000). Recession constant can be taken as the ratio of the baseflow at the time t to that of one day earlier (Nasimi, 2018).

$$Q_t = Q_0 k^t \qquad [3\text{-}3]$$

where Q_0 is the initial baseflow, Q_t is the baseflow at time t, and k is the exponential decay (recession) constant.

Nasimi (2018) analyzed recession parameters in the Hanwella watershed and found recession constant (k) and ratio to peak value as 1.006 and 0.138, respectively. Here the same values are applied for all sub-watersheds as an initial value and their final values are obtained through calibration.

3.4.2.5 Transform Method

Snyder Unit Hydrograph method is selected to convert excess precipitation into runoff since it provides satisfactory results in an ungauged, watershed with medium-sized watersheds (Chow et al., 1988). The method is based on linearity assumption, and its main parameters are basin lag time and the peak of the unit hydrograph. HEC-HMS requires basin lag time and peaking coefficient to be defined for this method. Peaking coefficient (C) and basin coefficient (C_t) are taken as 0.38, 3.75, respectively for the Kelani basin (Thapa & Wijesekera, 2017). Standard basin lag time was calculated according to Equation [3-4] (Chow et al., 1988).

$$t_l = 0.75\ C_t\ L\ L_c \qquad [3\text{-}4]$$

Where t_l is basin lag time in hours, C_t is basin coefficient, L is the longest flow path (from outlet to the watershed divide) in km, L_c is the distance from the outlet to the watershed centroid in km. The parameters L and L_c are derived for each sub-basin from HEC-HMS (sub-basin characteristics). The computed lag-time for each sub-basin is tabulated in Table 3-9.

Table 3-9: Calculation of Lag Time for Each Sub-basin

Sub-basin	longest Flow Path (km)	Centroidal Flow Path (km)	Basin Coefficient, Ct	Sub-basin lag, t_l (hr)
Kithulgala	59.75	29.97	3.75	26.61
Glencourse	58.67	17.00	3.75	22.32
Hanwella	73.64	37.44	3.75	30.28

3.4.2.6 Soil Moisture Accounting Loss Method

The Soil Moisture Accounting (SMA) loss method is selected as the loss method for the HEC-HMS model since this method is recommended for continuous simulation and provides satisfactory results (Nasimi, 2018). The initial values of all SMA parameters were estimated based on the literature (De Silva et al., 2013). A summary of the parameters with their initial values is tabulated in Table 3-10.

For the model calibration, ranges for some parameters of SMA was given according to the values shown in Table 3-11. Therefore, optimized values of these parameters should not fall out of these given ranges (Nasimi, 2018). These parameters were optimized while ensuring their values do not go beyond the given ranges.

Table 3-10: Initial Values of Soil Moisture Accounting Parameters Used for Model Calibration

Parameter	Value
Soil (%)	70
Ground water 1 (%)	45
Ground water 2 (%)	82
Maximum infiltration (mm/h)	10
Imperviousness (%)	40
Soil storage (mm)	125
Tension storage (mm)	75
Soil percolation (mm/h)	1
Ground water 1 storage (mm)	100
Ground water 1 percolation (mm/h)	1
Ground water 1 coefficient (hr)	100
Ground water 2 storage (mm)	150
Ground water 2 percolation (mm/h)	1
Ground water 2 coefficient (hr)	100

Source: (De Silva et al., 2013)

Table 3-11: Recommended Range of Some Soil Moisture Accounting Parameters Used for Parameter Optimization and Model Calibration

Parameters	Source	Range
Max infiltration (mm/h)	Saxton & Rawlas (2006); Gyawali (2013)	5 - 45
Tension storage (mm)	U.S. Army Corps of Engineers (USACE, 2010)	10 - 60
Soil percolation (mm/h)	WMS (1999); Gyawali (2013) Soil storage (mm) WMS (1999); Gyawali (2013)	0.05 - 5
Soil storage (mm)	WMS (1999); Gyawali (2013)	40-150

Source: (Nasimi, 2018)

3.4.2.7 Channel Routing

Channel routing is required to transfer hydrograph from the outlet of one sub-watershed to the other. HEC-HMS has eight different methods for channel routing (Gunathilake et al., 2019), from which the Muskingum routing method is extensively applied for flood routing (Song et al., 2011). The method requires two parameters, which are K and X. The parameter K defines the travel time through the reach, and the X parameter is the weighing between inflow and outflow influence, which ranges between 0 and 0.5 (Nasimi, 2018). Parameter X can be taken between 0.3 and 0.5 (Wijesekera & Rajapakse, 2013). Here 0.3 is selected for the parameter X since this value is used for natural streams. Parameter K can be estimated from channel length and flood wave velocity (USACE, 2021). Channel length for each sub-basin is obtained from demarcated streams in HEC-HMS, and flood wave velocity is estimated based on stream slope (Guideline from Irrigation Department). Calculated final values of K for each reach are tabulated in Table 3-12.

Table 3-12: Calculation of Travel Time (K) for Muskingum Routing

Reach	Length (km)	Average Slope (%)	Average Velocity (m/s)	Travel Time, K (hr)
Reach-1	32.17	0.11	0.46	19.55
Reach-2	27.17	0.07	0.46	16.51

3.4.2.8 Meteorology

In the meteorology component of HEC-HMS, different methods are available for meteorological input parameters. The required input parameter/data varies based on the method selected. Rainfall is introduced to the model using the gauge weights method. The depth weight of each gauge is determined by dividing the Theisen area of the gage by the corresponding area of the sub-watershed. The time weight for a given gauge is taken as 1 and 0 for gauges with the highest and lower weight, within a sub-watershed, respectively within a sub-watershed (HMS, 2000). Depth weight and time weight of each station are summarised in Table 3-13.

Table 3-13: Depth Weight and Time Weight of each Rain Gauge for the Corresponding Sub-basin

Station	Sub-basin	Area of the Gauge (m^2)	Depth Weight	Time Weight
Hanwella	Glencourse	1,765,730	0.003	0
Weweltalawa Estate	Glencourse	631,037,524	0.997	1
Hanwella	Hanwella	405,515,945	0.530	1
Laxapana	Hanwella	158,149,221	0.207	0
Weweltalawa Estate	Hanwella	200,755,180	0.263	0
Laxapana	Kithulgala	399,420,003	0.948	1
Weweltalawa Estate	Kithulgala	21,978,013	0.052	0

For the model calibration, evapotranspiration is modelled based on observed evapotranspiration data. However, in the case of climate model projections, evapotranspiration is modelled using daily minimum and maximum temperature, as other relevant data such as relative humidity and wind speed are not available. Since the Hargreaves method calculates evapotranspiration based on daily minimum and maximum temperature, it was chosen to model evapotranspiration (Equation [3-5]). The method is applied extensively, especially in the data-scarce watersheds as it models evapotranspiration with reasonable accuracy and minimal input data (Hargreaves & Allen, 2003).

$$PET = 0.0023\ R\ TD^{0.5}\ (TC + 17.8) \qquad [3\text{-}5]$$

where R is the incoming solar radiation at top of the atmosphere (in MJ m^{-2} day^{-1}), TD is the difference between the maximum and minimum daily temperatures, and TC is the average daily temperature in °C.

HEC-HMS can model evapotranspiration with the Hargreaves method when Hargreaves short wave is combined with Hargreaves evapotranspiration method. The shortwave coefficient and Hargreaves coefficient were given as default values in the model (0.1267 and 0.0135, respectively). Central meridian, which is required to determine the time zone, is specified at the watershed outlet (80.08^0 E). Additionally, HEC-HMS requires temperature time series to be in sub-daily intervals to analyze the daily temperature range (USACE, 2016). Therefore, daily minimum and maximum temperate were merged in HEC-DSS software to make them in the sub-daily interval.

3.5 Model Calibration and Validation

The HEC-HMS model was calibrated and validated for the dataset between 1997-2001 and 2002-2006. The model is calibrated and validated using daily streamflow at Hanwella station (outlet of the watershed), daily rainfall from Hanwella, Laxapana, and Weweltalawa Stations, and daily observed evapotranspiration from Colombo station. All the parameters were adjusted to minimize the difference between simulated and observed streamflow for the calibration. Parameters of different modelling components in HEC-HMS were adjusted using combined automatic, and semi-automatic calibration (manual changing parameters) approaches (Madhushankha & Wijesekera, 2021). The simplex search method was used in automatic calibration since it allows simultaneous change of multiple parameters (HMS, 2000). The Peak-weighted RMSE objective function was used as the statistics method since it provided better results than other available methods. Since this research focuses on simulating overall water balance rather than high flows or low flows, the Mean Ratio of Absolute Error (MRAE) is used as the primary objective function for calibrating the model. The MRAE performance metric is recommended when both high flows and low flows need to be captured by the model (Wijesekera & Abeynayake, 2003). Moreover, MRAE has been widely used across Sri Lanka for water resources assessment and it is also recommended by World Meteorological Organization (WMO) (Dissanayaka & Rajapakse, 2019; Nasimi, 2018; Sharifi, 2015).

In addition to MRAE, other performance criteria including Nash Sutcliffe Efficiency (NSE), Coefficient of Determination (R^2), and Pbias were also evaluated to further evaluate the performance of the model in terms of reproducing peaks and overestimation/underestimation of simulated streamflow (Nasimi, 2018; Samady, 2017). The recommended ranges of these performance criteria are given in Table 3-14.

Table 3-14: Recommended Range of Various Objective Functions

Performance rating	R2	PBIAS/PVE	NSE	MRAE
Very good	0.75< R2 ≤1	PBIAS≤±10	0.75<NSE≤1	0<MRAE<4
Good	0.65 <R2 ≤0.75	±10 ≤PBIAS <±15	0.65<NSE≤0.75	4<MRAE<5
Satisfactory	0.75< R2 ≤0.65	±15 ≤PBIAS <±25	0.50<NSE≤0.65	5<MRAE<7
Unacceptable	R2 ≤ 0.5	PBIAS≥±25	NSE≤0.5	MRAE>7

Source: (Nasimi, 2018)

3.6 Model Performance Metrics

There are numerous performance indicators used for different applications. The selection of a particular metric depends on the objective of modelling. For instance, when peak flow needs to be simulated accurately, higher values of NSE are recommended. Since this research focuses on general water balance, MRAE and Pbias are the primary metrics for calibrating the model. In addition to these two indicators, other indicators (NSE and R^2) are also evaluated to check the model performance in reproducing peak flows and the existence of a correlation between observed and simulated streamflow. These objective functions with their corresponding formula are presented as follows.

The Nash Sutcliffe Efficiency (NSE) is a well-known performance metric widely used in calibrating/validating a hydrologic model, especially when peak flows are of concern. It determines the relative error in the variance of simulated discharge compared to the observed one. The NSE values lie between -∝ and 1. Values close to 1 imply good calibration while a value below 0.5 is not acceptable. The indicator can be calculated by Equation [3-6]. In all equations, Q_{obs}, Q_{sim}, and $\overline{Q_{obs}}$ stands for observed, simulated, and the average of observed streamflow, respectively.

$$NSE = 1 - \frac{\sum(Q_{sim} - Q_{obs})^2}{\sum(Q_{obs} - \overline{Q_{obs}})^2} \qquad [3\text{-}6]$$

Pbias performance indicator shows the model capability to simulate total runoff volume (World Bank DC., 2015). The simulated discharge is overestimated when it is positive or vice versa. The lower the value of Pbias (close to zero) implies good performance. This indicator is calculated using Equation [3-7].

$$Pbias\,(\%) = \frac{\sum(Q_{obs} - Q_{sim})}{\sum Q_{obs}} \times 100 \qquad [3\text{-}7]$$

Coefficient of Determination (R^2) indicates whether the model's variation of observed data is captured (Mahmood et al., 2016). The ideal value for this indicator is 1; any value above 0.65 can be classified as acceptable (Nasimi, 2018). When the values are close to 1, there is a good correlation between the observed and simulated data. The performance metric can be calculated using Equation [3-8].

$$R^2 = \frac{\sum(Q_{obs} - \overline{Q_{obs}}) \times \sum(Q_{sim} - \overline{Q_{sim}})}{\sqrt{\sum(Q_{obs} - \overline{Q_{obs}})^2} \times \sqrt{\sum(Q_{sim} - \overline{Q_{sim}})^2}} \qquad [3\text{-}8]$$

Many researchers use the Mean Ratio of Absolute Error (MRAE) for water resources assessment (Dissanayaka & Rajapakse, 2019; Nasimi, 2018; Sharifi, 2015). This indicator shows the difference between simulated and observed streamflow concerning the observation under consideration (Nasimi, 2018). The optimum values for this objective function are close to zero. The indicator is calculated using Equation [3-9], where n shows the total number of observations.

$$MRAE = \frac{1}{n}\sum\left|\frac{Q_{obs} - Q_{sim}}{Q_{obs}}\right| \qquad [3\text{-}9]$$

CHAPTER 4

4 RESULTS

This chapter provides details on the results and analysis part of the research. The contents of the chapter encompass the assessment of bias-corrected data, calibrated, and validated model, change of hydrometeorological parameters (e.g., precipitation, temperature, and streamflow) from the historical period (1985-2014) to the projected mid-century (2030-2059) and later-century periods (2070-2099) under SPP2-4.5 and SSP4-8.5 climate scenarios. Changes in hydrometeorological parameters are evaluated under various temporal scales – daily, monthly, and seasonal. This chapter mainly focuses on streamflow variation, and much of the trend analysis is performed to identify the properties of projected streamflow. The overall water balance, and hydrologic extreme, including drought and flood, are analyzed for projection periods and scenarios.

4.1 Evaluation of Bias-Corrected Data

4.1.1 Evaluation of Bias-Corrected Precipitation

Observed, GCM derived, and bias-corrected GCM time series for the whole historical period (1985-2014) are considered for evaluation. It should be noted that observed data refers to daily observed precipitation at the Hanwella Gauging station, and GCM data is the output from the CNRM-CM6-1 model. To assess the performance of this bias-correction method for precipitation, various statistics are calculated and tabulated in Table 4-1. According to the statistics, the mean and the sum of observed data are equal to that of bias-corrected data, indicating a good shift from GCM data to bias-corrected one. On the other hand, quartiles (25^{th}, 50^{th}, and 75^{th} percentile) of bias-corrected data reveal an overestimation of precipitation, while the maximum rainfalls are underestimated. The objective functions listed in Table 4-2 are calculated to assess bias correction's overall performance. A good performance of bias-corrected data is observed as Pbias is zero compared to GCM-derived data. NSE and Pbias performance criteria show slightly good performance of the corrected data.

Table 4-1: Statistical Comparison of Observed, Raw and Bias Corrected Precipitation – Monthly Data

Statistics	Precipitation (mm)		
	Observed	GCM-Derived	Bias-Corrected (Linear Scaling)
Mean	262.73	197.91	262.73
Variance	32,283.85	16,864.30	24,556.32
Sum	94,582.84	71,246.29	94,582.84
Min	0.00	0.00	0.00
25^{th} Percentile	122.68	89.83	150.52
50^{th} Percentile	236.15	195.99	246.83
75^{th} Percentile	367.35	285.86	371.77
Max	899.07	591.10	771.15

Table 4-2: Determination of Objective Functions for Observed, GCM Rainfall and Bias Corrected Data – Monthly Data

Performance Criteria	GCM Rainfall	Bias-Corrected GCM Rainfall
NSE	-0.16	-0.12
R^2	0.34	0.37
Pbias (%)	-24.67	0.00

Considering the monthly distribution of each time series through box plots (Figure 4-1), observed precipitation shows a higher variation compared to raw and bias corrected ones. For most of the months, GCM data is significantly lower than observed data (Pbias is -24 %), indicating clear bias of the data from the climate model.

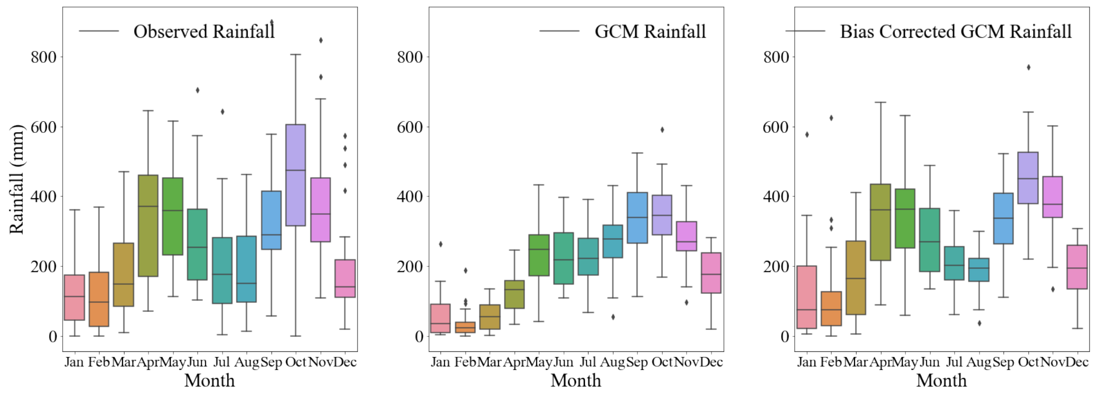

Figure 4-1: Boxplot of Monthly Rainfall for Observed, Raw and Bias Corrected Rainfall – Daily Data

Figure 4-2 shows a scatter plot for GCM-derived (Figure 4-2a) and bias-corrected GCM (Figure 4-2b) rainfall. The straight line shows regression line, which shows the the degree of correlation between x and y axes. When the line has slope of 1 (45^0), it means perfect correlation between x and y. In the case of GCM rainfall, the lower region is underestimated, which is corrected quite well after applying bias correction. Good performance of bias-corrected data can also be seen in the normal distribution plot (Figure 4-3a) and cumulative probability (Figure 4-3b) plots. Most GCM-derived rainfall is significantly lower than observed and bias-corrected data (bias of -24%), as indicated in the cumulative probability plots. Further, bias-corrected data are underestimated for high rainfall values, while the medium and lower rainfall values show a good match with observed data.

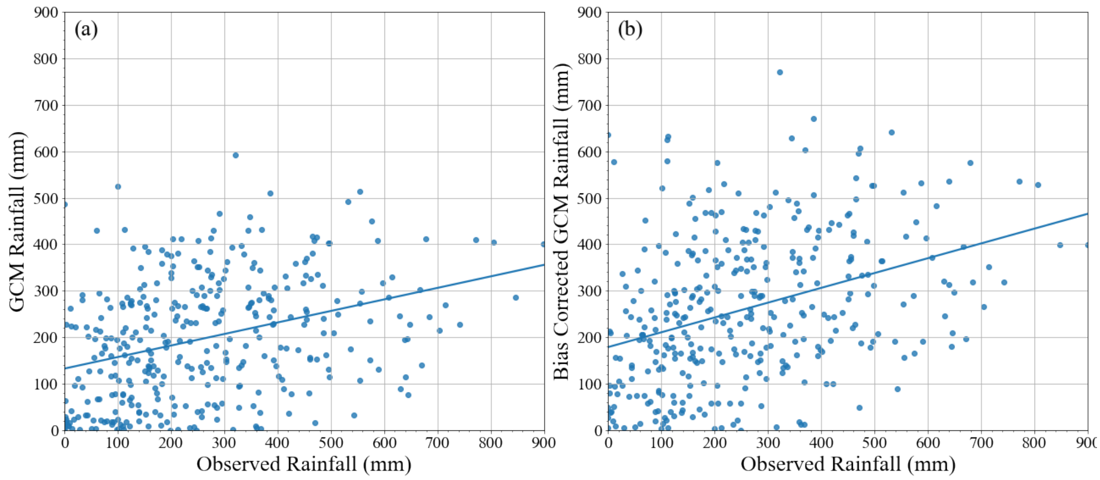

Figure 4-2:Scatter Plot for GCM vs. Observed Precipitation (a) and Bias Corrected GCM vs. Observed Precipitation (b) – Monthly Data

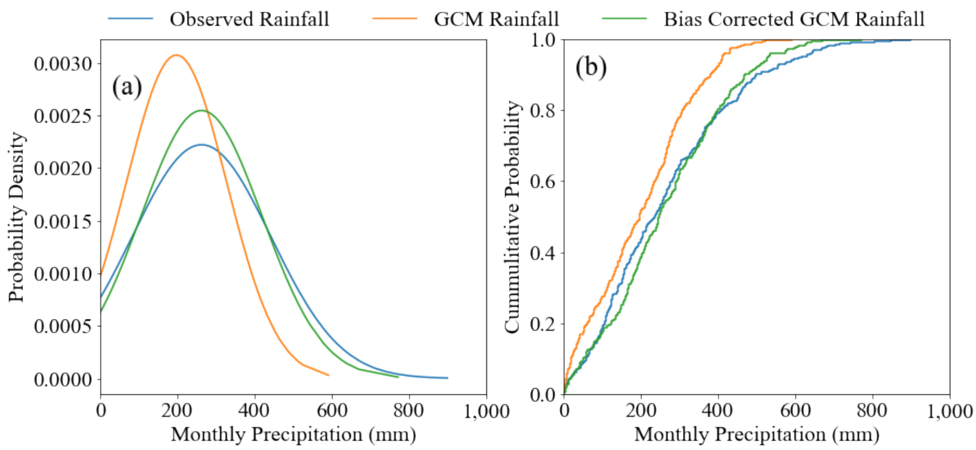

Figure 4-3: Probability Density Function (a) and Cumulative Distribution Function (b) for Observed, GCM, and Bias Corrected Precipitation – Monthly Data

4.1.2 Evaluation of Bias-Corrected Minimum Temperature

Only the minimum temperature of the Colombo gauging station is considered to evaluate bias-corrected temperature data. Similar to the evaluation of bias-correction of precipitation data, various statistics of minimum temperature are calculated and tabulated in Table 4-3. Observed, GCM, and bias-corrected GCM time series from the CNRM-CM6-1 model for the whole historical period (1985-2014) is considered for analysis. According to the statistics, the mean of observed data is equal to that of bias-corrected data. On the other hand, quartiles (25^{th}, 50^{th} percentile, and maximum) of bias-corrected data closely match with observed data, indicating a good shift of GCM-derived data.

Table 4-3: Statistical Comparison of Observed, GCM-derived and Bias-Corrected Minimum Temperature – Monthly Data

Statistics	Minimum Temperature (^{0}C)		
	Observed	GCM-derived	Bias Corrected (Variance Scaling)
Mean	24.70	24.38	24.70
Variance	1.43	0.65	1.65
Min	21.79	22.55	21.57
25^{th} Percentile	23.77	23.78	23.71
50^{th} Percentile	24.84	24.31	24.74
75^{th} Percentile	25.65	24.98	25.63
Max	27.34	26.61	28.46

Considering the monthly distribution of each time series through box plots (Figure 4-4), bias-corrected and observed minimum temperature shows a higher variation (0-28 ^{0}C) than GCM-derived data (0-26 ^{0}C). GCM-derived data is slightly lower than observed and bias-corrected data for most months (April-November).

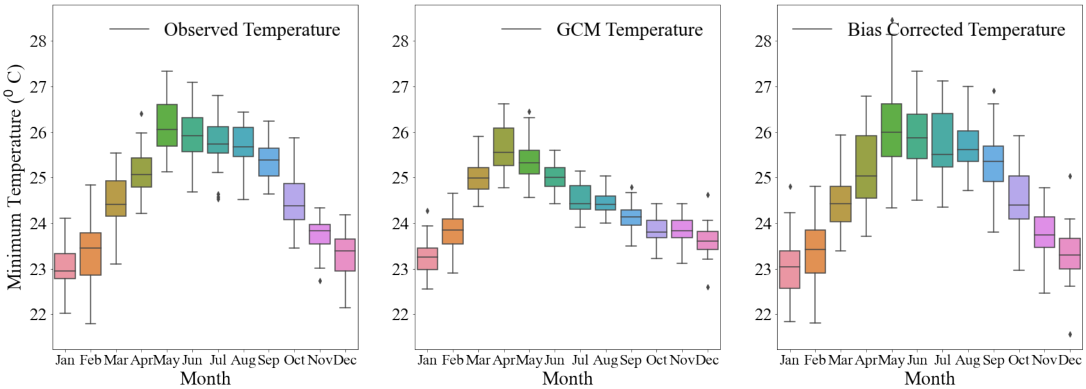

Figure 4-4: Boxplot of Mean Monthly Minimum Temperature of Observed, GCM-derived, and Bias Corrected Data – Daily Data

Figure 4-5 shows a scatter plot for GCM-derived (Figure 4-5a) and bias-corrected GCM (Figure 4-5b) minimum temperature values. The straight line shows regression line, which shows the the degree of correlation between x and y axes. When the line has slope of 1 (45^{0}), it means perfect correlation between x and y. GCM-derived data underestimate the higher region of temperature, which is corrected reasonably through bias correction. However, bias corrected data slightly overestimate lower temperature values. A similar conclusion can be drawn from probability distribution (Figure 4-6a) and cumulative distribution (Figure 4-6b) plots as well.

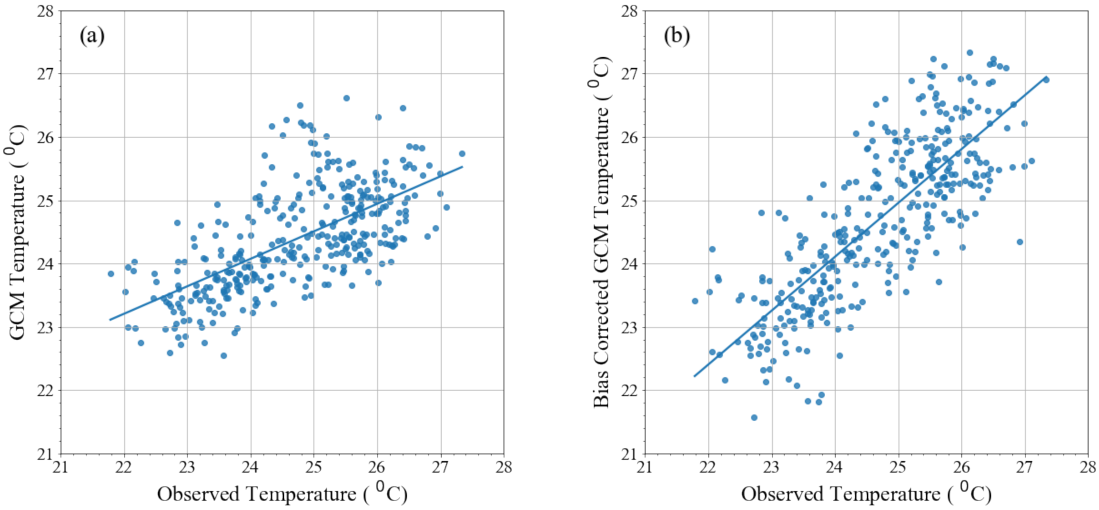

Figure 4-5: Scatter Plot for GCM vs. Observed Minimum Temperature (a) and Bias Corrected vs. Observed Minimum Temperature (b) – Monthly Data

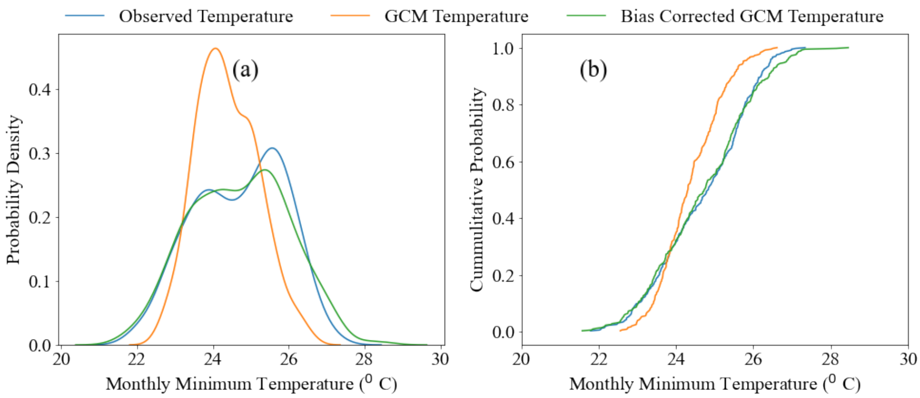

Figure 4-6: Probability Distribution Function (a) and Cumulative Probability Distribution (b) for Observed, GCM, and Bias Corrected Minimum Temperature – Mean Monthly Data

4.2 HEC-HMS Model Performance in Calibration and Validation

4.2.1 Evaluation of Calibrated and Validated Model – Daily Data

The model's performance for both calibration (1997-2001) and validation (2002-2006) is assessed under the daily time scale. Table 4-4 summarizes the calculated objective functions for the given calibration and validation periods. The remark columns indicate the category that these objective functions belong to, as recommended in Table 3-14. All the specified objective functions show satisfactory results. The model simulates overall water balance quite well as Pbias and R^2 are 1.63% 0.83, respectively during calibration, while it overestimates flow during validation (Pbias of 12.24%). Peak flows are simulated relatively well during calibration and validation with NSE of 0.68 and 0.67, respectively. Low flows are simulated relatively better during calibration (MRAE of 0.54) than validation (MRAE of 0.63).

Additionally, graphs are plotted to further assess model performance during the calibration and validation. Figure 4-7 indicates observed and simulated streamflow with their respective flow duration curve in the annual timescale. The figure reveals the cyclic pattern of variation in streamflow and rainfall. The seasonal trend also matches, where the Maha and Yala seasons are the rainy seasons with a high discharge volume. Streamflow in the medium range is simulated well, while high flows are somewhat underestimated, and low flows are overestimated.

Table 4-4: Objective Functions for the Model Calibration (1997-2001) and Validation (2002-2006) – Daily Data

Performance Criteria	Calibration	Remarks	Validation	Remarks
NSE	0.68	Good	0.67	Good
Pbias (%)	1.63	Very Good	12.24	Good
R^2	0.83	Very Good	0.83	Very Good
MRAE	0.54	Very Good	0.63	Very Good

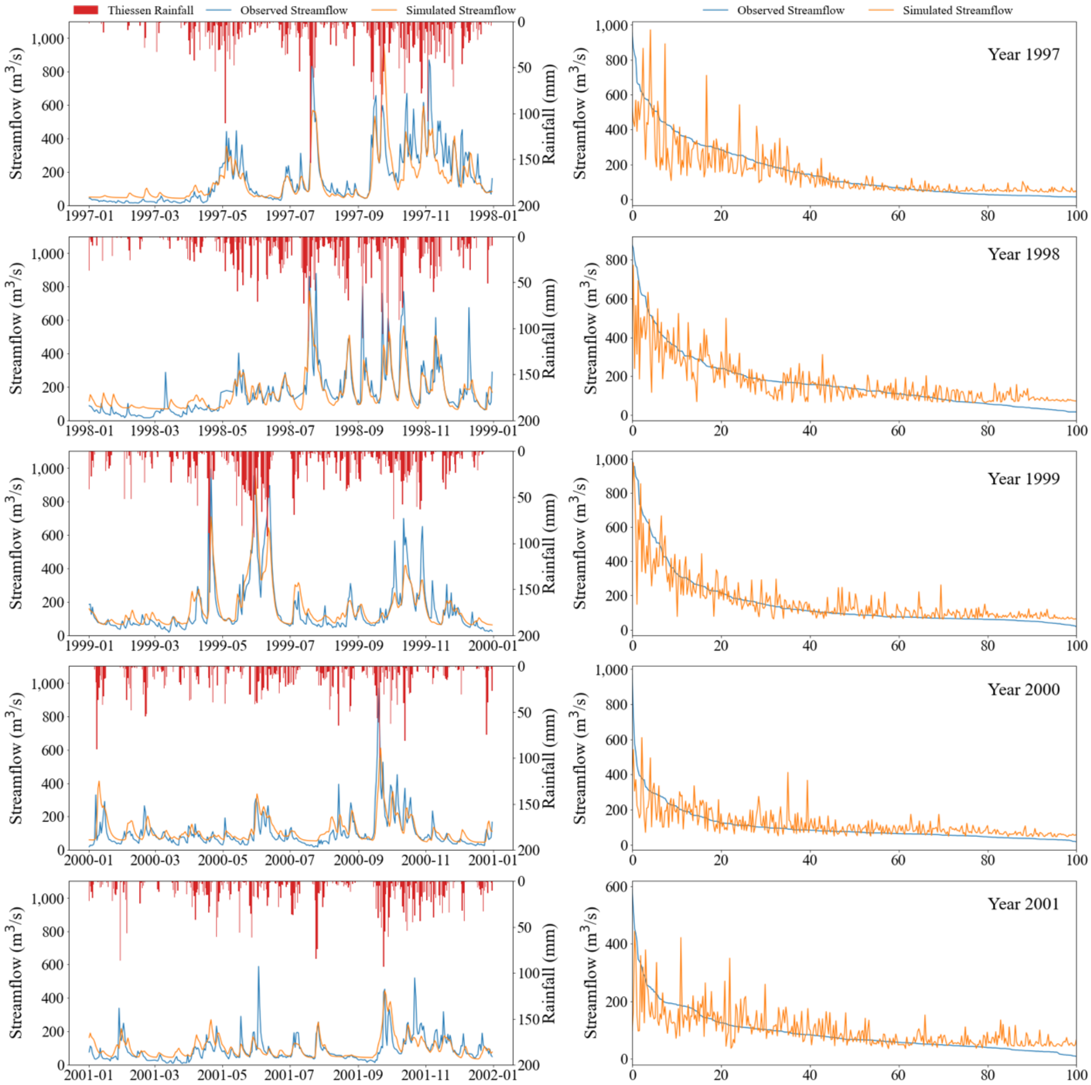

Figure 4-7: Simulated and Observed Streamflow with Their Corresponding Flow Duration Curve in Annual Interval during Model Calibration – Daily Data

Figure 4-8 shows observed and simulated streamflow (in normal and log scales) and Theisen rainfall during the model calibration. Simulated/observed streamflow reveals an apparent correlation with rainfall time series. The visual examination shows a satisfactory performance of simulated discharge, noting that extreme high flows are underestimated while low flows are overestimated.

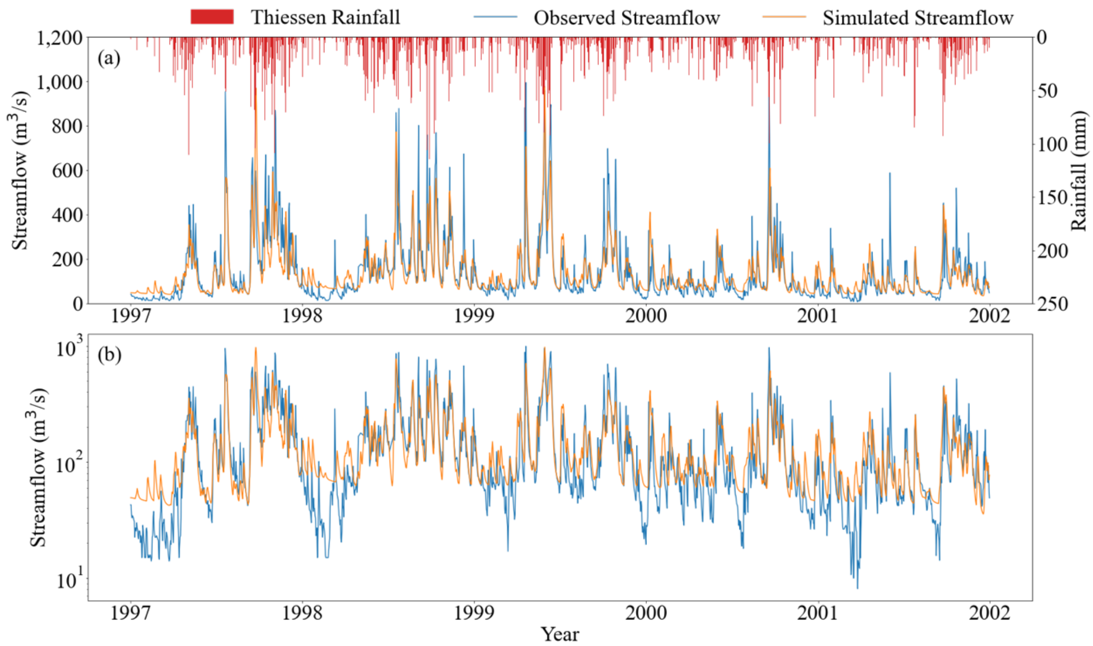

Figure 4-8: Simulated and Observed Streamflow for the Calibration Period (1997-2001) – Normal (a) and Semi-Log (b) Plots, Daily Data

Figure 4-9 shows the flow duration curve for observed and simulated streamflow (in normal and log scales) during the model calibration. Low flows are overestimated, while high flows are underestimated. The model simulates streamflow quite well within the 20-60 % probability of exceedance range. Further, the model shows good performance in simulating high flows compared to low flows.

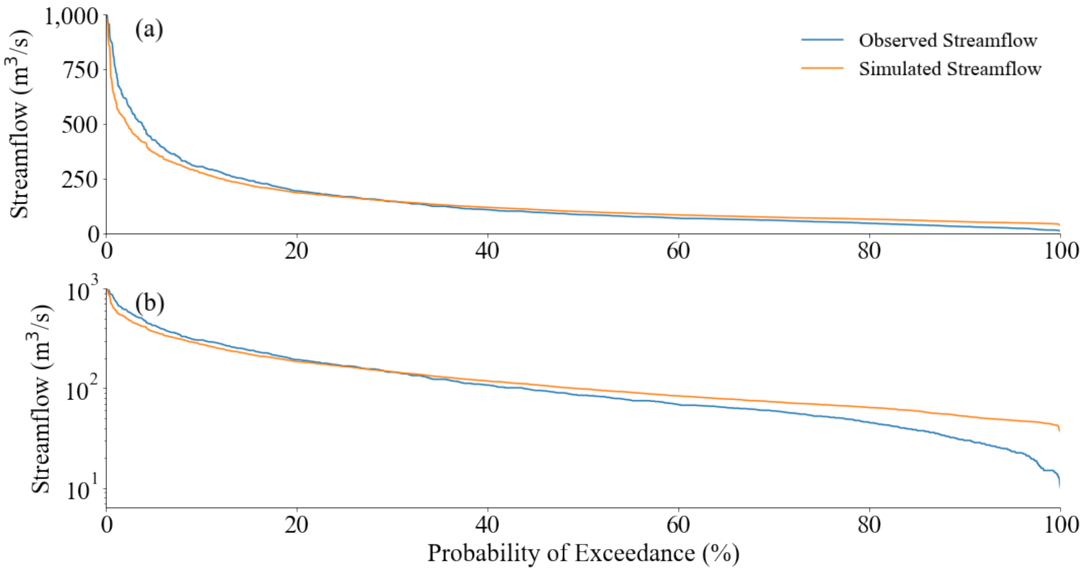

Figure 4-9: Simulated and Observed Streamflow Flow Duration Curve for the Calibration Period (1997-2001) – Normal (a) and Semi-Log (b) Plots, Daily Data

Figure 4-10 shows observed and simulated streamflow (in normal and log scales) and Theisen rainfall during the model validation. Simulated/observed streamflow reveals an apparent correlation with rainfall time series. The overestimation of low flows is slightly higher in 2004 and 2006, while the remaining years show an acceptable simulation of the low streamflow region. The visual examination shows a satisfactory performance of simulated discharge.

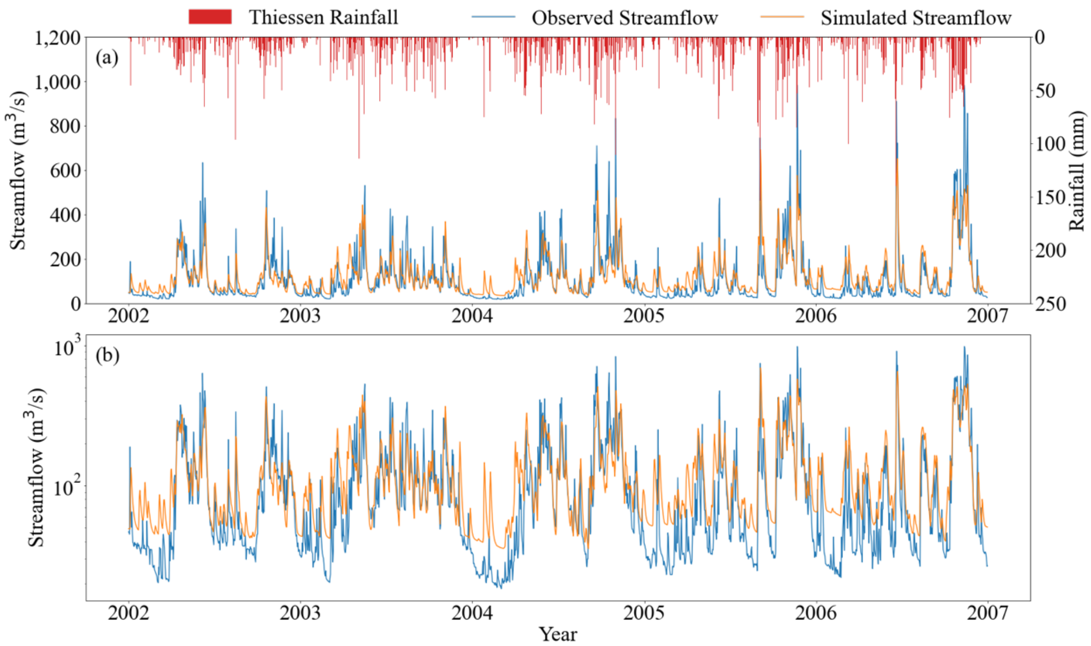

Figure 4-10: Simulated and Observed Streamflow for the Validation Period (2002-2006) – Normal (a) and Semi-Log (b) Plots, Daily Data

Figure 4-11 shows the flow duration curve for observed and simulated streamflow (in normal and log scales) during the model validation. Low flows are overestimated, while high flows are underestimated. The model simulates streamflow quite well in the range of 0-40 % probability of exceedance. Further, the model shows good performance in simulating high flows compared to low flows.

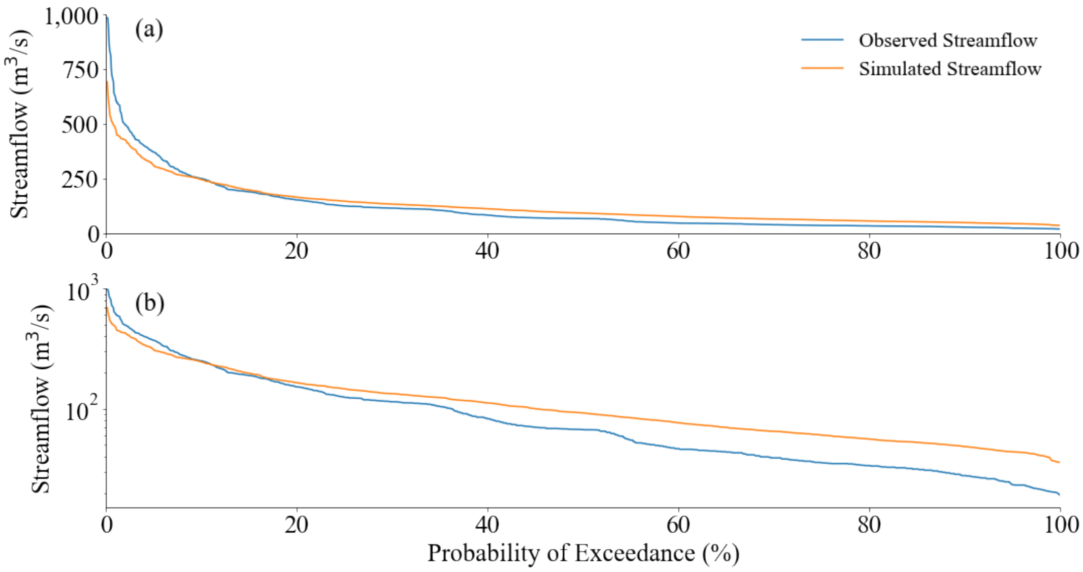

Figure 4-11:Simulated and Observed Streamflow Flow Duration Curve for the Validation Period (2002-2006) – Normal (a) and Semi-Log (b) Plots, Daily Data

4.2.2 Evaluation of Calibrated and Validated Model – Monthly Data

The model's performance for both calibration (1997-2001) and validation (2002-2006) is also assessed under the monthly time scale. Table 4-5 summarizes calculated objective functions for the calibration and validation periods. The remark columns indicate the category that these objective functions fall, as recommended in Table 3-14. All the specified objective functions show satisfactory results. The model simulates overall water balance quite well as Pbias and R^2 are 1.74% 0.93, respectively, during calibration, while it overestimates flow during validation (Pbias is 12.24%). Peak flows are simulated relatively well during calibration and validation with NSE of 0.85 and 0.77, respectively. Low flows are simulated relatively well during calibration (MRAE of 0.33) compared to validation (MRAE of 0.43).

Table 4-5: Objective Functions for the Model Calibration (1997-2001) and Validation (2002-2006) – Monthly Data

Performance Criteria	Calibration	Remarks	Validation	Remarks
NSE	0.85	Very Good	0.77	Very Good
Pbias	1.74	Very Good	12.24	Good
R^2	0.93	Very Good	0.91	Very Good
MRAE	0.33	Very Good	0.43	Very Good

Figure 4-12 shows observed and simulated monthly streamflow during the model calibration and validation. The overestimation of low flows is high during model validation (2004, 2005, and 2006). On the other hand, simulated high flows reveal slight underestimation. The model's overall performance is satisfactory since the simulated streamflow follows the observed streamflow pattern.

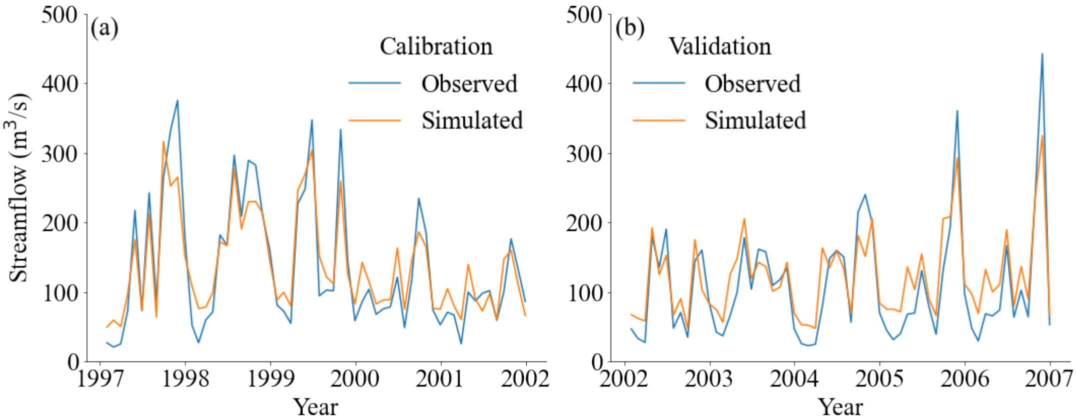

Figure 4-12: Observed and Simulated Streamflow during Model Calibration (a) and Validation (b) – Monthly Data

4.3 Change in Climate

Change in hydrometeorological parameters, including daily and monthly precipitation, minimum and maximum temperature (i.e., Tmin, Tmax) are determined to evaluate the trend of projected parameters versus historical time series under the given projected scenarios of SSPs 2-4.5 and 5-8.5. It is to be noted that the change in precipitation is evaluated by averaging relevant time series across all the rain gauge stations. In the case of Tmin and Tmax, time series from the Colombo temperature gauging station is considered, as it was the only available gauge.

4.3.1 Change in Precipitation

4.3.1.1 Change of Precipitation at Annual Time Scale

Changes in annual rainfall for the projected and historical periods are analyzed by calculating the mean of daily precipitation in each year and the corresponding period (Figure 4-13). This evaluation shows increasing precipitation intensity under SSPs 2-4.5 and 5-8.5 except the EARTH model. Further, the annual changes (range from -500 to 2,000 mm) are significantly higher than seasonal changes (range from -200 to 1,200 mm) (Figure 4-15). Further, according to ensemble projections, the late-century period shows a higher increase (600-800 mm) than the mid-century (400-600 mm). In the model ensemble, higher changes are expected under SSP5-8.5 (500-800 mm) than SSP2-4.5 (400-600 mm). Moreover, SSP5-8.5 reveals a range of fluctuation for different models.

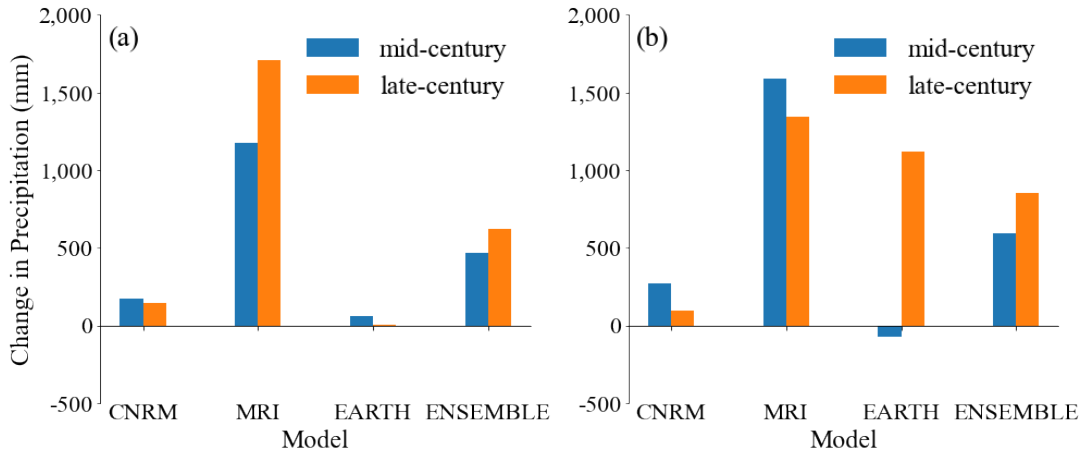

Figure 4-13: Change in Inter-Annual Precipitation under SSP2-4.5 (a) and SSP5-8.5 (b) for Mid-Century (2030-2059) and Late-Century (2070-2099) concerning Reference Period (1985-2014)

4.3.1.2 Change of Precipitation in Monthly Time Scale

Figure 4-14 shows the changes in monthly precipitation for designated projection periods and scenarios, which range between -80 to 250 mm. A higher rainfall variation can be seen in SSP5-8.5 (-80 to 250 mm) compared to SSP2-4.5 (-80 to 200 mm). The late century has higher changes than the mid-century period for both scenarios. Comparison of monthly change suggests that months of January to May would experience decreasing rainfall, while the rest of the months are projected to have increased precipitation, with the increase being significantly pronounced during June to Septemper (100-250 mm). This conclusion can be drawn for both scenarios and periods. The results of monthly changes are somewhat similar to the findings of Shrestha et al. (2013), which has reported increasing precipitation for May-October, and decreasing trend for November to April months.

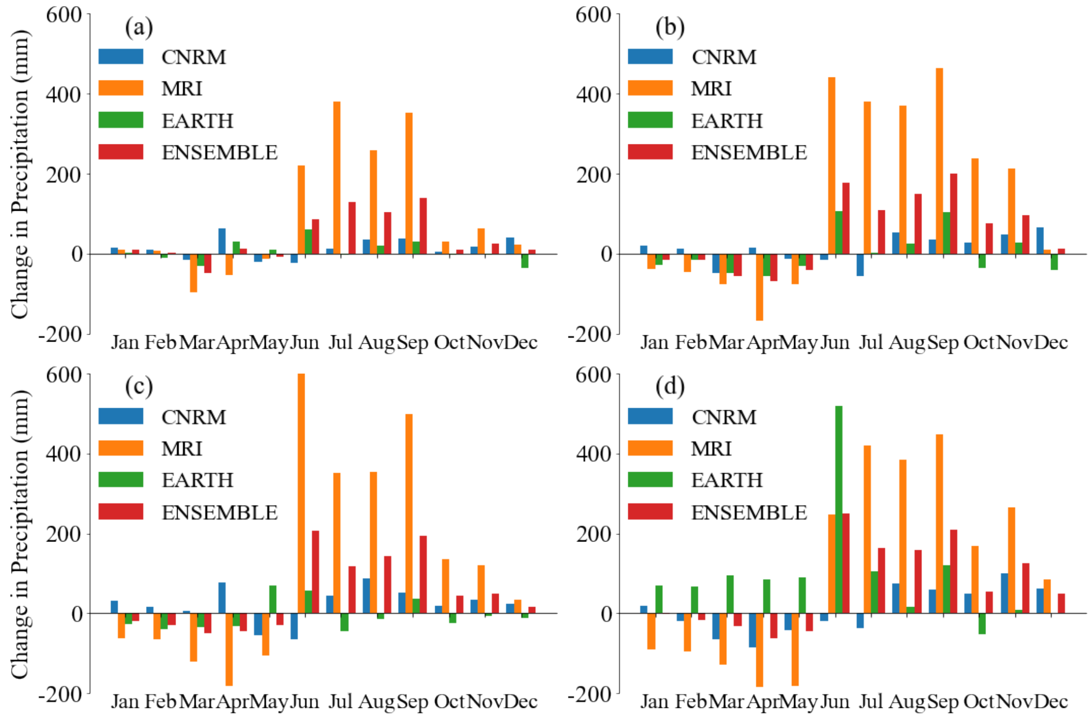

Figure 4-14: Change in Monthly Precipitation under SSP2-4.5 (a and b) and SSP5-8.5 (c and d) for Mid-Century (a and c) Period (2030-2059) and Late-Century (b and d) Period (2070-2099) concerning Reference Period (1985-2014)

4.3.1.3 Change of Precipitation at Seasonal Time Scale

Figure 4-15 shows the changes in seasonal precipitation for designated projection periods and scenarios. A higher rainfall variation can be seen in SSP5-8.5 (-100 to 700 mm) compared to SSP2-4.5. In both scenarios, the late-century has higher changes (range in between -180 to 700 mm) than the mid-century (range in between -100 to 600 mm) with the model ensemble. Comparison of seasonal changes shows drier season (First Inter-Monsoon) has the lowest reduction (30-180 mm) while wetter season (Southwest Monsoon) has the highest increase (around 400-700 mm). Other seasons indicate a slight increase/decrease in precipitations. Studies found similar results from Southeast Asia (Mekong Basin), which has reported increasing precipitation mainly in the wet season (May-October), and a decreasing trend in the dry season (November to April) (Shrestha et al., 2013).

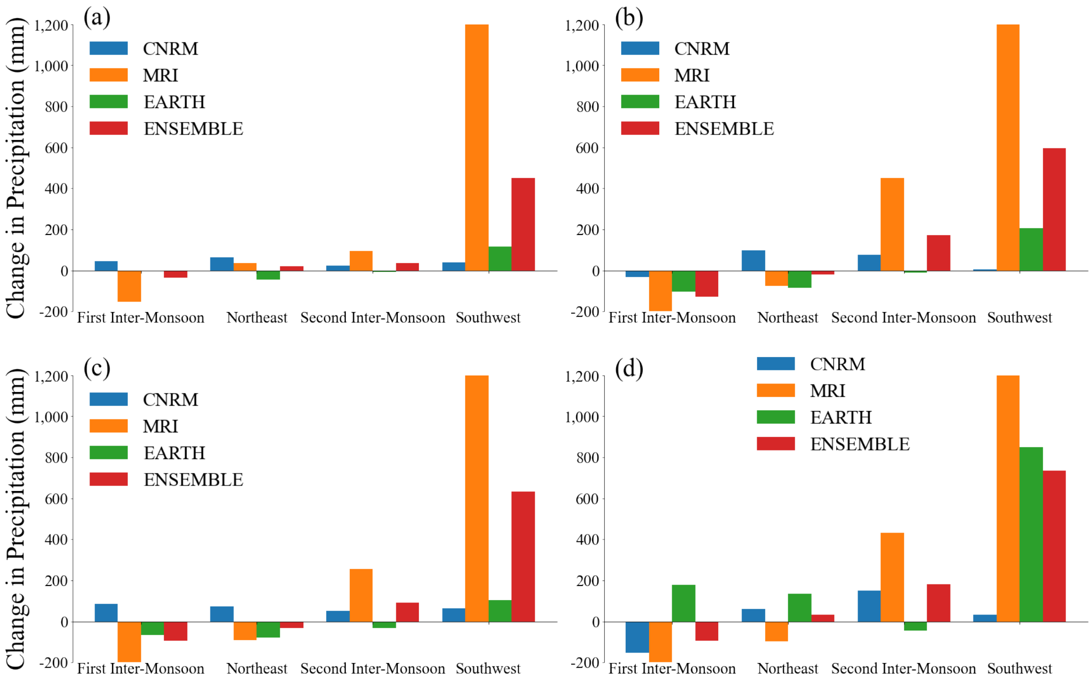

Figure 4-15: Change in Seasonal Precipitation under SSP2-4.5 (a and b) and SSP5-8.5 (c and d) for Mid-Century (a and c) Period (2030-2059) and Late-Century (b and d) Period (2070-2099) concerning (1985-2014)

4.3.2 Change in Minimum Temperature

4.3.2.1 Change of Minimum Temperature at Annual Time Scale

Figure 4-16 shows increasing minimum temperature under both SSPs 2-4.5 and 5-8.5, with a higher increase under SSP5-8.5. Further, the late-century period shows higher changes (2-4 ^{0}C) than mid-century (1-2 ^{0}C). CNRM indicates the highest changes (1-4 ^{0}C) while MRI shows the least changes (0.5-3 ^{0}C) in minimum temperature for all scenarios and periods. Changes in minimum temperature are slightly higher (2-4 ^{0}C) than maximum temperature (2-3 ^{0}C) in the late century. (Figure 4-19). Other studies found similar results with consistently increasing temperature and significantly higher temperature change toward the late-century period (Gunathilake et al., 2020; Tanteliniaina et al., 2021).

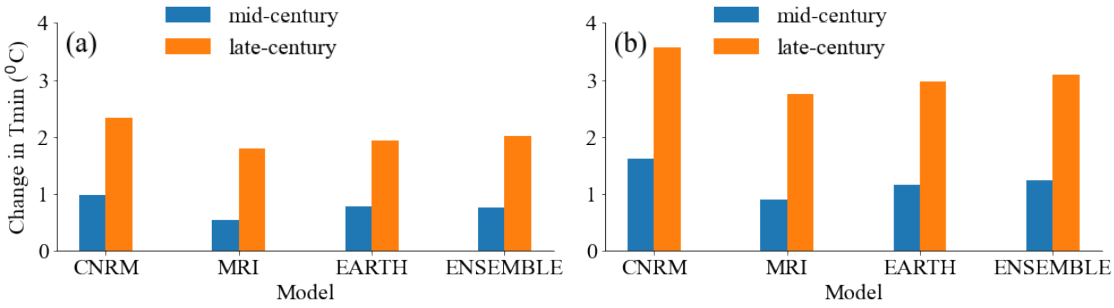

Figure 4-16: Change in Mean Annual Minimum Temperature (T_{min}) under SSP2-4.5 (a) and SSP5-8.5 (b) for Mid-Century (2030-2059) and Late-Century (2070-2099) concerning Reference Period (1985-2014)

4.3.2.2 Change of Minimum Temperature in Monthly Time Scale

Figure 4-17 shows changes in monthly minimum temperature for designated projection periods and scenarios. In both scenarios, the late-century period has higher changes (2-4 ^{0}C) than the mid-century period (1-2 ^{0}C). Comparison of monthly changes shows that April to July has higher changes (1-4 ^{0}C) while September to November has smaller changes (0.5-3 ^{0}C) than other months. This conclusion can be drawn for both scenarios and periods.

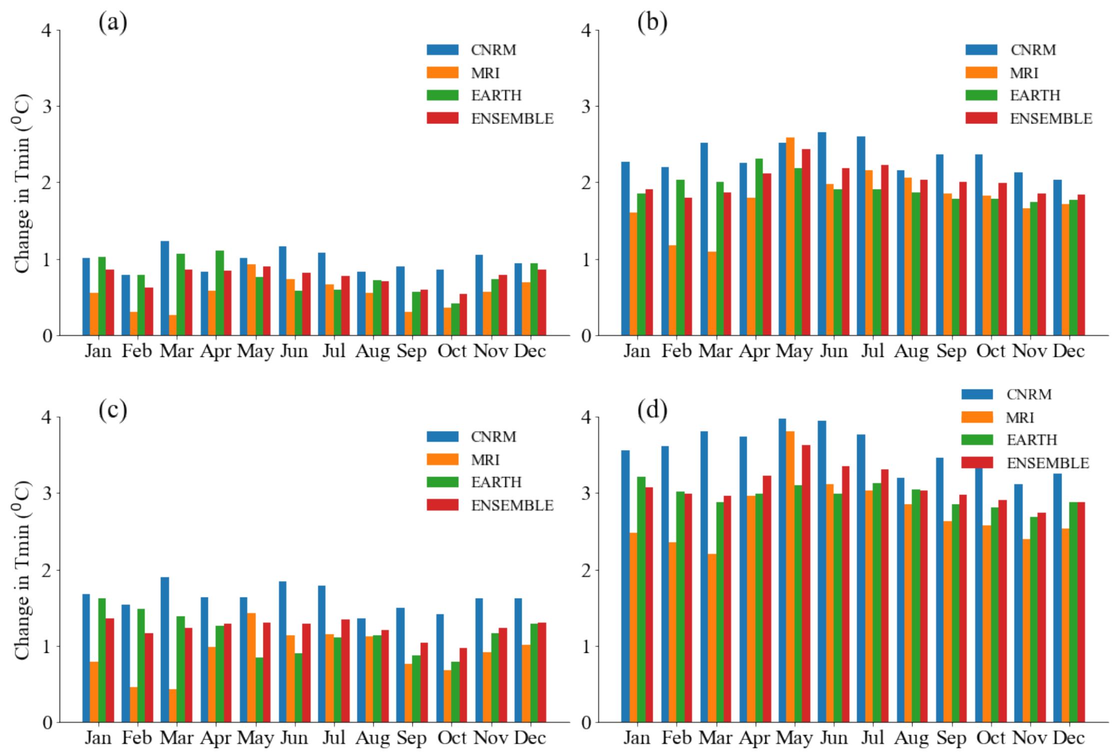

Figure 4-17: Change in Monthly Minimum Temperature (T_{min}) under SSP2-4.5 (a and b) and SSP5-8.5 (c and d) for Mid-Century (a and c) Period (2030-2059) and Late-Century (b and d) Period (2070-2099) concerning Reference Period (1985-2014)

4.3.2.3 Change of Minimum Temperature in Seasonal Time Scale

Figure 4-18 shows changes in seasonal minimum temperature for designated projection periods and scenarios. In both scenarios, the late-century period has higher changes (2-4 ^{0}C) than the mid-century (1-2 ^{0}C). Comparison of seasonal changes shows no clear distinction between each season. All seasons follow a similar pattern of changes in minimum temperature.

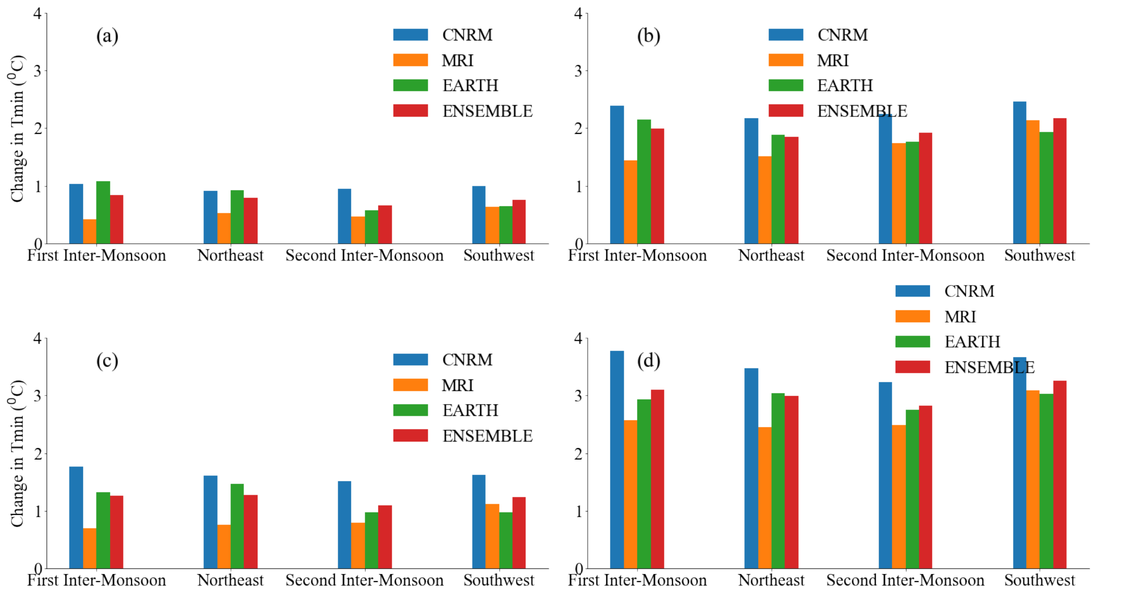

Figure 4-18: Change in Seasonal Minimum Temperature (T_{min}) under SSP2-4.5 (a and b) and SSP5-8.5 (c and d) for Mid-Century (a and c) Period (2030-2059) and Late-Century (b and d) Period (2070-2099) concerning Reference Period (1985-2014)

4.3.3 Change in Maximum Temperature

4.3.3.1 Change of Maximum Temperature in Annual Time Scale

Figure 4-19 shows increasing maximum temperature under both SSPs 2-4.5 and 5-8.5. Further, the late-century period shows higher changes (2-4 ^{0}C) than that of the mid-century (1-2 ^{0}C). CNRM indicates the highest changes (1.2-3.3 ^{0}C) while MRI shows the least changes (1-2.8 ^{0}C) in maximum temperature for all scenarios and periods.

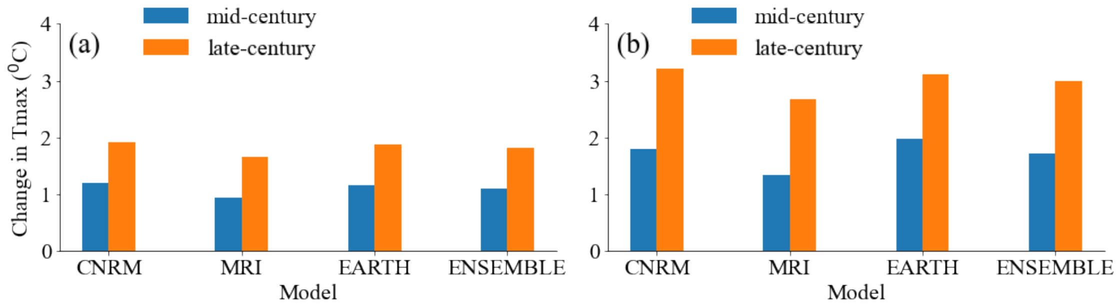

Figure 4-19: Change in Mean Annual Maximum Temperature (T_{max}) under SSP2-4.5 (a) and SSP5-8.5 (b) for Mid-Century (2030-2059) and Late-Century (2070-2099) concerning Reference Period (1985-2014)

4.3.3.2 Change of Maximum Temperature at Monthly Time Scale

Figure 4-20 shows the changes in monthly maximum temperature for the selected projection periods and scenarios. In both scenarios, the late-century period has higher changes (2-4 ^{0}C) than the mid-century (1-2 ^{0}C). Comparison of monthly changes shows that January, February, and December have higher changes (1-4 ^{0}C) while August, September, and October have small changes (1-3 ^{0}C) than other months during the late-century period.

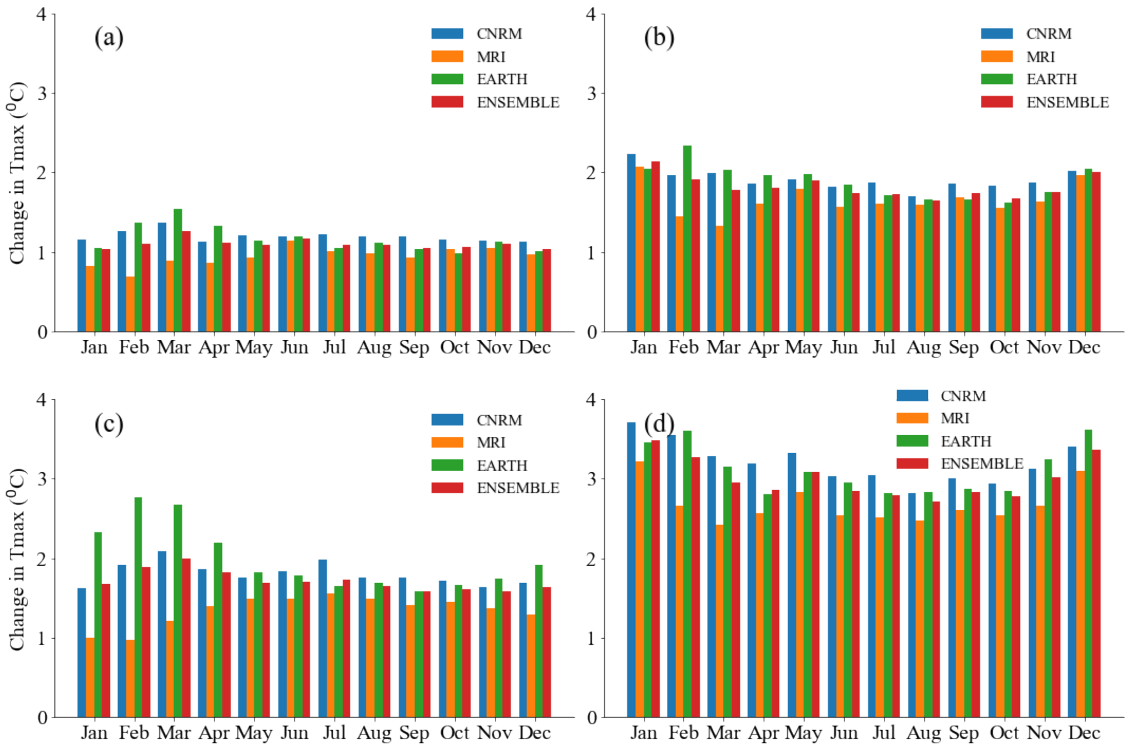

Figure 4-20: Change in Monthly Maximum Temperature (T_{max}) under SSP2-4.5 (a and b) and SSP5-8.5 (c and d) for Mid-Century (a and c) Period (2030-2059) and Late-Century (b and d) Period (2070-2099) concerning Reference Period (1985-2014)

4.3.3.3 Change of Maximum Temperature at Seasonal Time Scale

Figure 4-21 shows the changes in maximum seasonal temperature for the selected projection periods and scenarios. In both scenarios, late-century has higher changes (2-4 ^{0}C) than mid-century (1-2 ^{0}C). Comparison of changes in each season shows highest changes during First Inter-Monson (1.5-3 ^{0}C) and Northeast Monsoon (1.5-3.5 ^{0}C) in the late century and mid-century, respectively, under both scenarios.

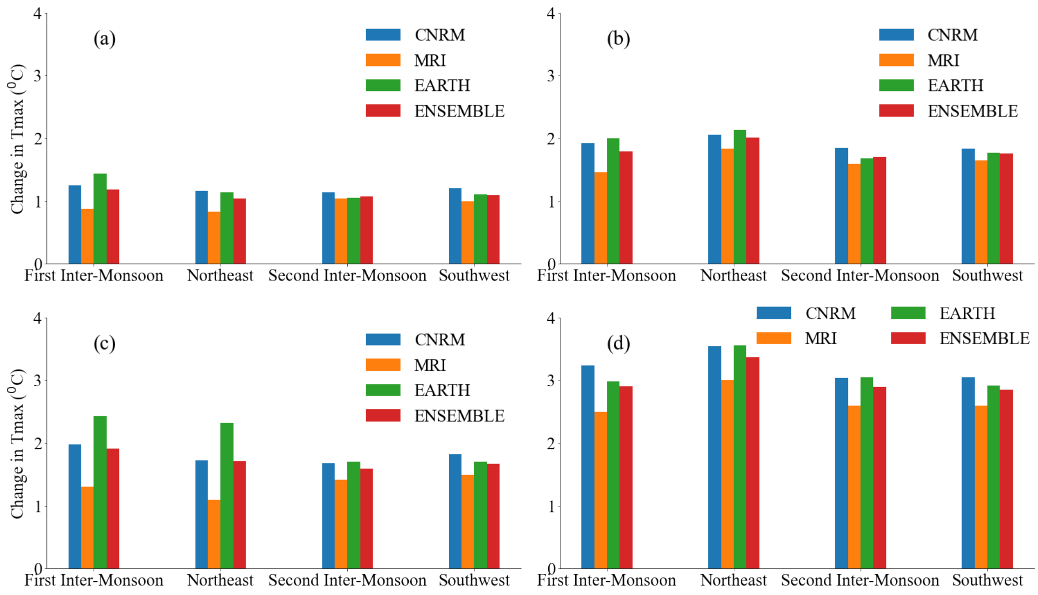

Figure 4-21: Change in Seasonal Maximum Temperature (T_{max}) under SSP2-4.5 (a and b) and SSP5-8.5 (c and d) for Mid-Century (a and c) Period (2030-2059) and Late-Century (b and d) Period (2070-2099) concerning Reference Period (1985-2014)

4.4 Change in Hydrology

4.4.1 Change of Streamflow at Annual Time Scale

Changes in mean annual streamflow for the projected and historical periods (Figure 4-22) show increasing streamflow under both SSPs 2-4.5 and 5-8.5, except the EARTH model. Further, according to ensemble inputs driven model results, the late-century period shows higher changes (range between 25-40 m^3/s) than mid-century (range between 15-25 m^3/s). Further, inter-annual changes in projected streamflow suggest smaller changes (-25 to 100 m^3/s) than monthly changes (-50 to 300 m^3/s) (Figure 4-23) and seasonal changes (-50 to 200 m^3/s) (Figure 4-24) in river discharges, considering all the models. These changes may be attributed to the complex and contrasting sub-basin changes in precipitation and evaporation (Shrestha et al., 2013). Moreover, the changes in rainfall and streamflow for the CNRM model do not have a reasonable correlation (Figure 4-22). Changes in rainfall show a higher increase under SSP5-8.5 toward the late century (Figure 4-13). However, the streamflow change of this model does not show a significant increase. This is because of the same model projects significantly high temperatures in the late century. As a result, river discharge can decrease. The inter-annual changes from previous studies also suggest increasing river flows (Shrestha et al., 2013; Zhang et al., 2018), similar to this study's findings.

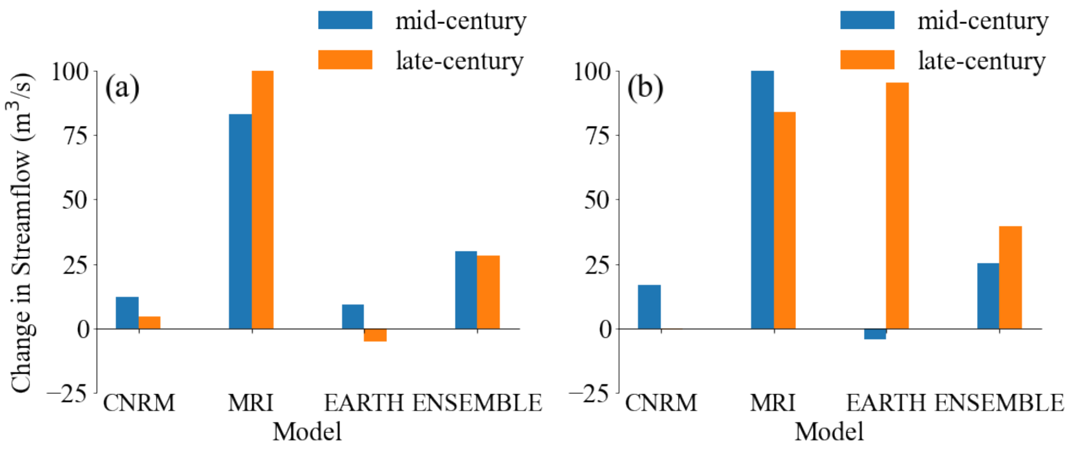

Figure 4-22: Change in Mean Annual Streamflow under SSP2-4.5 (a) and SSP5-8.5 (b) for Mid-Century (2030-2059) and Late-Century (2070-2099) concerning Reference Period (1985-2014)

4.4.2 Change of Streamflow at Monthly Time Scale

Figure 4-23 shows the changes in monthly mean streamflow over the selected projection periods and scenarios. Generally, rainy months (June-December) indicate significantly higher changes (25-100 m^3/s), while January-May reveals a variable change (-10 to 25 m^3/s) in streamflow with a higher chance of decreasing trend for both scenarios and periods, as indicated by ensemble model. The changes for wet months are significant under both scenarios in the late century (20-100 m^3/s) compared to mid-century (20-80 m^3/s). Further, changes are high under SSP5-8.5 (-10 to 100 m^3/s) than SSP2-4.5 (-10 to 70 m^3/s). Changes in October and November become more noticeable toward the late-century period under both scenarios (40-60 m^3/s). Comparison of monthly change suggests that June and September have the highest changes (40-100 m^3/s), with the projected increases becoming large (50-100 m^3/s) towards the late-century period of both scenarios. The same months are projected to have the highest increment in rainfall (Figure 4-14), which would result in such changes in projected streamflow.

Additionally, the findings closely agree with studies from Koshi Basin in Nepal that reported increasing flow during wet months (June and July) (Devkota & Gyawali, 2015). The point to be noted is that changes in streamflow on a monthly scale are significantly high compared to seasonal and inter-annual changes. Therefore, it is recommended to use monthly streamflow to plan and manage water resources in the basin (Shrestha et al., 2013).

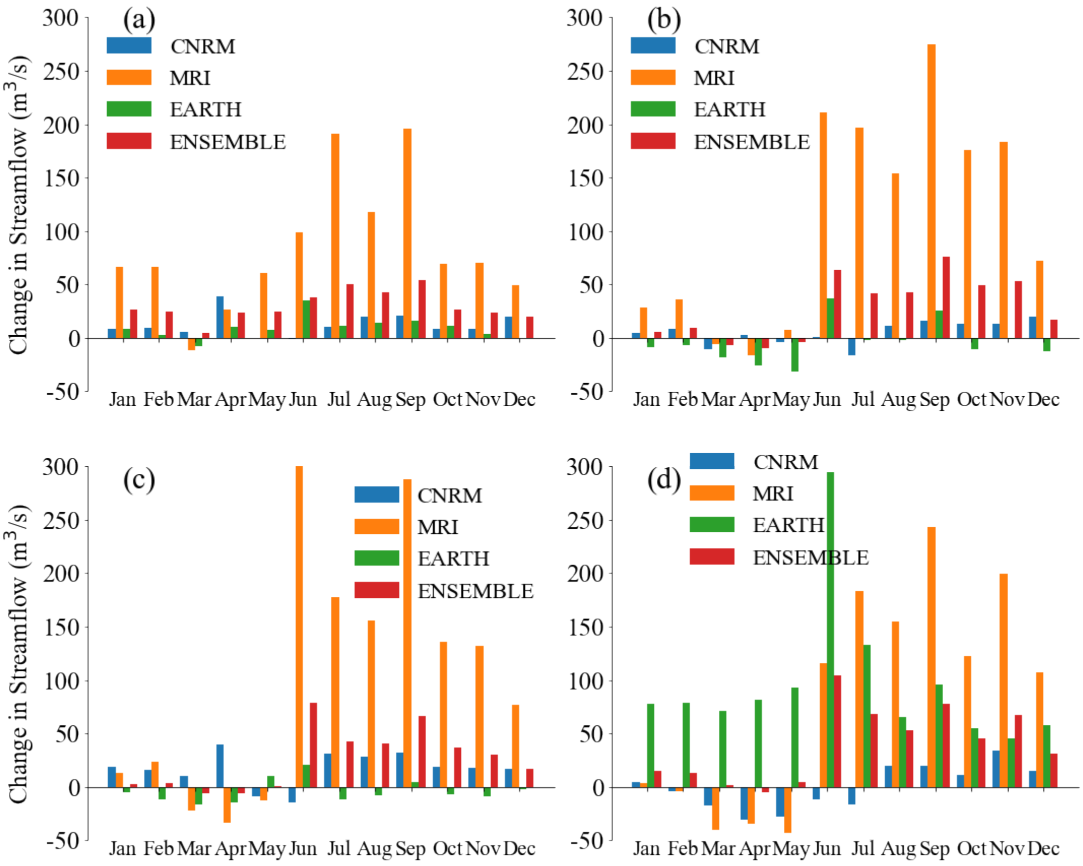

Figure 4-23: Change in Mean Monthly Streamflow under SSP2-4.5 (a and b) and SSP5-8.5 (c and d) for Mid-Century (a and c) Period (2030-2059) and Late-Century (b and d) Period (2070-2099) concerning Reference Period (1985-2014)

4.4.3 Change of Streamflow at Seasonal Time Scale

Figure 4-24 shows the changes in mean seasonal streamflow for the selected projection periods and scenarios. Comparison of seasonal change shows increasing streamflow for the Southwest, Second-Inter, and Northeast Monsoon in incremental order. However, the First-Inter Monsson (dry season) reveals decreasing trend except for the mid-century under SSP2-4.5. Further, the projected changes of the ensemble derived model are significant for the Southwest and Second-Inter Monsoons (40 to 60 m^3/s) during the late-century period. Previous studies from Southeast Asia show a high change in streamflow in the wet season (Shrestha et al., 2013), which substantiate the findings fo this study.

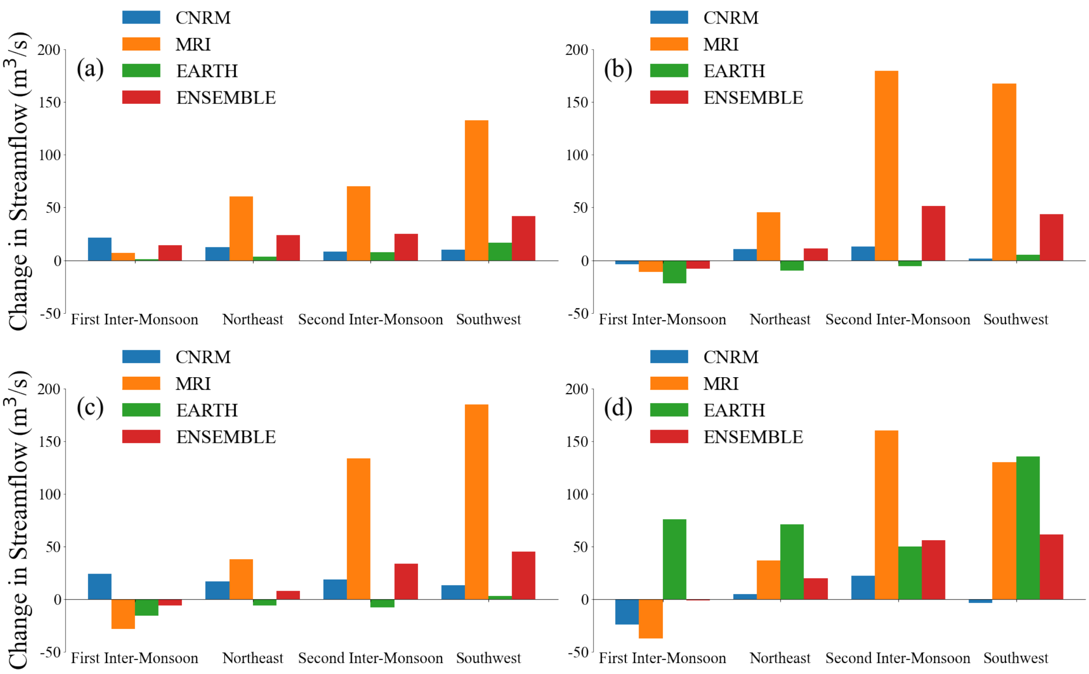

Figure 4-24: Change in Mean Seasonal Streamflow under SSP2-4.5 (a and b) and SSP5-8.5 (c and d) for Mid-Century (a and c) Period (2030-2059) and Late-Century (b and d) Period (2070-2099) concerning Reference Period (1985-2014)

4.4.4 Change in Extreme Streamflow

Changes in extreme and median streamflows are analyzed using Flow Duration Curve (FDC), Probability Density Function (PDF), and Cumulative Distribution Function (CDF). Moreover, using 95%, 50%, and 5% values of FDC, streamflow is classified into high (Q_5), median (Q_{50}), and low (Q_{95}), respectively (Mahmood et al., 2016). The changes in each streamflow categories are quantified for the projected periods concerning the baseline period.

The streamflow categories for historical and projected periods of each model under both scenarios are tabulated in Table 4-6. Different streamflow categories indicate various high/low values. The MRI model generally shows the highest values in different streamflow regions (38-805 m^3/s), while EARTH reveals the least discharge different streamflow regions (19-487 m^3/s). The CRNM projections rank in the medium range compared to MRI and CNRM.

Additionally, changes in each streamflow categories are quantified for the projected periods and scenarios concerning reference period (Table 4-7). All the models project increasing high, median, and low flows except CNRM and EARTH. The EARTH model shows a decreasing pattern, especially for median and low flows during the mid-century and end-century periods under SSP5-8.5 and SSP2-4.5, respectively. Based on the ensemble inputs derived model projections, high flows show a higher increase (19-30%) than the median (19-26%) and low flows (16-30%) except for SSP2-4.5 mid-century. All models project significantly high changes in high (30%), low (30%), and median flows (26%) in the late century under SSP5-8.5. The result of this analysis is different from previous findings of the studies from other parts of the world. Specifically, Gunathilake et al. (2020) evaluated projected streamflow from three RCMs of CORDEX in the Nan River Basin, Thailand, under RCP 4.5 and 8.5. The projected changes in streamflow were assessed for future periods in 2020–2039 (2030s), 2040–2069 (2050s), and 2070–2099 concerning the base period (1988–2005). The findings suggest a decrease in high flows while an increase in low flows under both scenarios considered. Mahmood et al. (2016) investigated streamflow changes in Kunhar River basin, Pakistan. Change in streamflow was evaluated for future periods (2011–2040, 2041–2070, and 2071–2099) concerning the baseline period (1961–1990) under the A2 and B2 scenarios of the HadCM3 global climate model. The results suggest increasing median and high flows while decreasing low flows.

Table 4-6: Streamflow Classification Based on Flow Duration Curve (High (Q5)), Median (Q50), and Low Flows (Q95)) under the Corresponding Scenarios and Models for the Historical (1985-2014), Mid-Century (2030-2059), and Late-Century Period (2070-2099)

Period and Scenario	Streamflow Category	Model			
		CNRM	MRI	EARTH	ensemble
Historical	Q_5 (m^3/s)	306.50	459.40	259.40	224.60
	Q_{50} (m^3/s)	88.50	107.90	88.60	85.90
	Q_{95} (m^3/s)	29.80	38.80	22.70	24.50
SSP2-4.5 Mid-Century	Q_5 (m^3/s)	316.60	685.70	270.80	277.70
	Q_{50} (m^3/s)	100.50	161.20	96.50	115.60
	Q_{95} (m^3/s)	34.30	53.10	19.90	32.20
SSP5-8.5 Mid-Century	Q_5 (m^3/s)	328.70	778.50	255.80	280.30
	Q_{50} (m^3/s)	104.40	168.90	85.40	106.70
	Q_{95} (m^3/s)	36.40	55.40	20.50	29.30
SSP2-4.5 Late-Century	Q_5 (m^3/s)	289.70	805.90	261.60	297.00
	Q_{50} (m^3/s)	97.70	164.30	83.60	109.80
	Q_{95} (m^3/s)	33.10	68.30	18.70	31.70
SSP5-8.5 Late-Century	Q_5 (m^3/s)	304.70	751.30	486.70	322.80
	Q_{50} (m^3/s)	89.80	142.30	163.20	116.20
	Q_{95} (m^3/s)	27.10	57.60	41.60	34.90

Table 4-7: Change in Streamflow Categories (High (Q5)), Median (Q50), and Low Flows (Q95)) under the Corresponding Scenarios and Models for the Mid-Century (2030-2059) and Late-Century Period (2070-2099) Concerning Reference Period (1985-2014)

Period and Scenario	Change in Streamflow Category	Model			
		CNRM	MRI	EARTH	ensemble
SSP2-4.5 Mid-Century	Q_5 (%)	3.19	33.00	4.21	19.12
	Q_{50} (%)	11.94	33.06	8.19	25.69
	Q_{95} (%)	13.12	26.93	-14.07	23.91
SSP5-8.5 Mid-Century	Q_5 (%)	6.75	40.99	-1.41	19.87
	Q_{50} (%)	15.23	36.12	-3.75	19.49
	Q_{95} (%)	18.13	29.96	-10.73	16.38
SSP2-4.5 Late-Century	Q_5 (%)	-5.80	43.00	0.84	24.38
	Q_{50} (%)	9.42	34.33	-5.98	21.77
	Q_{95} (%)	9.97	43.19	-21.39	22.71
SSP5-8.5 Late-Century	Q_5 (%)	-0.59	38.85	46.70	30.42
	Q_{50} (%)	1.45	24.17	45.71	26.08
	Q_{95} (%)	-9.96	32.64	45.43	29.80

The historical and projected streamflows under both scenarios for all the models are visualized with FDC (Figure 4-25), PDF, and CDF (Figure 4-26). Analysis of streamflow reveals a significant increase in the late century under SSP5-8.5, especially the high region streamflow which can be distinguished in all the CDF plots in Figure 4-26.

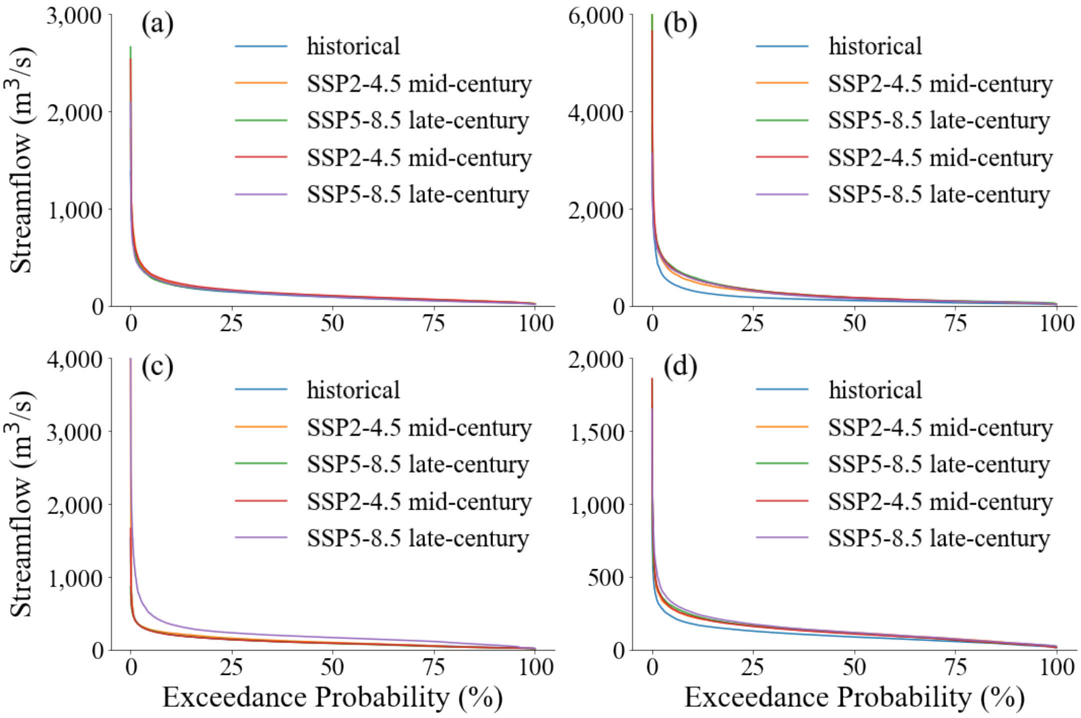

Figure 4-25: Flow Duration Curve for CNRM (a), MRI (b), EARTH (c), and Ensemble Model (d) for the Historical (1985-2014), Mid-Century (2030-2059), and Late-Century Period (2070-2099) under SSP2-4.5 and SSP5-8.5

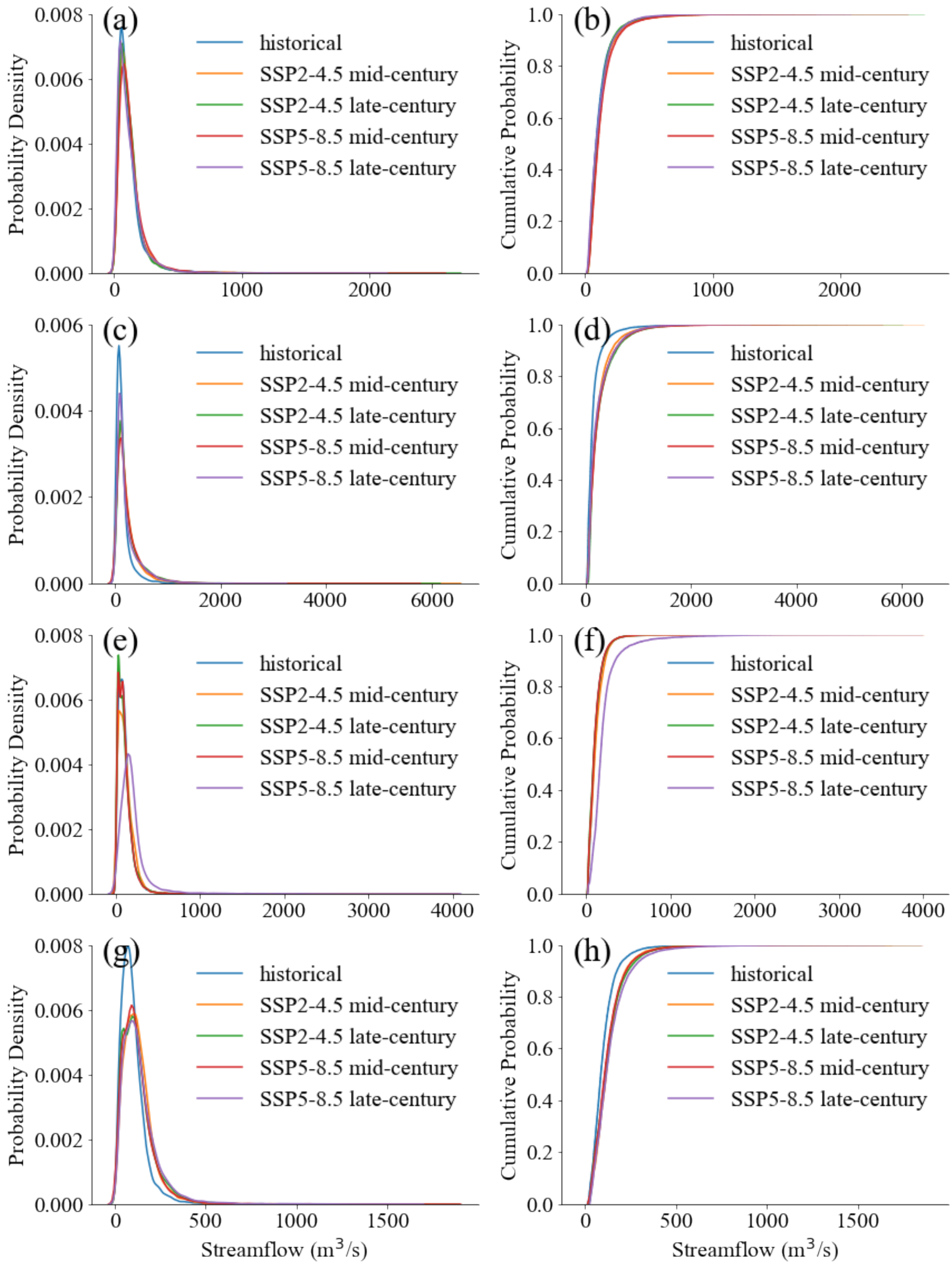

Figure 4-26: Probability Density Function with its Corresponding Cumulative Distribution Function for CNRM (a and b), MRI (c and d), EARTH (e and f), and Ensemble Model (g and h) for the Historical (1985-2014), Mid-Century (2030-2059), and Late-Century Period (2070-2099) under SSP2-4.5 and SSP5-8.5

CHAPTER 5

5 DISCUSSION

5.1 Change in Climate

Changes in rainfall suggested variable trends, while temperature changes were always unidirectional and consistently increasing for all projected periods and scenarios, with a more pronounced change in the late century. In general, an increasing precipitation trend was observed under both scenario and future periods. However, many other researchers' findings reveal decreasing precipitation in the near future while increasing trends in the long term (Gunathilake et al., 2020; Tanteliniaina et al., 2021). The reason behind this might be the small-time interval between mid-century and late-century considered in this study compared to the previous studies. Additionally, GCMs, without being downscaled, cannot capture local variability in precipitation due to their coarse resolution. Since the short-term precipitation has been reported to be highly variable, it can be another source of uncertainty in the projection of short-term precipitation.

This study's results have shown high temperature and rainfall changes, with significantly high changes in the late-century period. Other researchers found increasing precipitation under increasing temperatures towards the end-century period (Zhang et al., 2018). Moreover, changes in rainfall and temperature were high in the high emission scenario (SSP5-8.5) compared to low emission (SSP2-4.5), which is in agreement with previous studies (Mehrad, 2020; Tanteliniaina et al., 2021). Additionally, temperature projections under SSP5-8.5 suggest a significant increase.

The highest decrease in rainfall and maximum increase in maximum temperature was observed in the Firs-Inter Monsoon. Therefore, high intensity of droughts may occur during this season because the increasing temperature causes even further reduction in streamflow because of increased evapotranspiration. The high-temperature change can also influence rainfall patterns and intensity (Gunathilake et al., 2020).

5.2 Change in Hydrology

Streamflow is an essential component of the hydrologic cycle and plays vital role in a watershed. Proper monitoring and understanding of streamflow would better manage frequent natural disasters, including floods, drought, and other water quality issues. Therefore, analysis and management of streamflow can significantly help in water resources management. Many factors influence the streamflow regime (e.g., land use, soil, and climate change impact). Among these factors, climate change impact is the most dominant one, and its impact on streamflow variation has been extensively studied worldwide (Shrestha et al., 2013; Tanteliniaina et al., 2021; Gunathilake et al., 2020; Shreshtha et al., 2016). Further, understanding how the frequency and intensity of the extremes might change under changing climate is getting significant attention.

Under the given scenarios, streamflow changes for projected periods suggest an overall increasing trend in average annual streamflow, ranging between 20-25 m^3/s and 25-40 m^3/s for the mid-century and late-century periods of the ensemble-driven model outputs, respectively). The changes in streamflow correlate with that of rainfall, but it is not the same because of the nonlinear relation between streamflow and rainfall. Further, the model that projects high-temperature changes (CNRM) shows slightly less changes in discharges than rainfall changes, especially during the late-century period. This can occur because temperature increase can lead to more evapotranspiration, thus reducing the water availability/river flow (Tian et al., 2016).

Comparison of streamflow changes at different time scales reveals the highest change in the monthly analysis when compared to the seasonal and annual changes. A similar result was reported by Shrestha et al. (2013), where change in streamflow from Nam Ou basin located in northern Laos was evaluated using four general circulation models and a regional circulation model (PRECIS). Therefore, it is essential to consider the monthly streamflow for water resources planning and management in the the Kelani River Basin. Moreover, wet months/seasons (especially the Southwest Monsoon) indicate a significant increase in streamflow, while an opposite trend is projected for dry season (First-Inter Monsoon), noting exception for the mid-century SSP2-4.5. In this view, seasonal floods and droughts occurrence are expected to exacerbate in future.

The changes of seasonal streamflow suggest a significant increase during rainy seasons (Southwest and Second-Inter Monsoon), which can be attributed to the high increase in the rainfall volume for the same season. However, studies from Southeast Asia project decreasing streamflow with a more pronounced decrease in the rainy seasons (Gunathilake et al., 2020; Shrestha et al., 2022). Further, different streamflow categories (i.e., high, median, and low flows) revealed an increasing trend with a more pronounced high flow region increase than low and median flows. Changes for the high, median, and low flows range between 19 - 30%, 19 - 26%, and 16 - 30%, respectively. Since the precipitation analysis showed a significant high change in the rainy monsoon seasons, the high region of streamflow can experience high change as the basin is normally experiencing high flows during rainy Monsoon seasons.

5.3 Study's Limitations

In this study variability in streamflow is studied under climate change impact and given sceanarios. However, many other factors, including land use change, influence hydrology and streamflow regime. Given the scope of this research and time constrained, this study only considered climate change impact on streamflow.

For land use projections, several tools are available. These tools/models are calibrated and validated based on historical data, then they are used for forecasting land use. Though these models provide reliable results in short term future they may not simulate long-term changes in land use with reasonable accuracy (Wang et al., 2021). On the other hand, this study's aim is to evaluate long-term changes in streamflow.

Additionally, the study's aim was to evaluate overall water balance rather than peak flows. Land use change has significant impact on peak flows compared to general streamflow trend (Kundu & Olang, 2011). Given the aforementioned limitations, the impact of land use changes on streamflow is not considered here.

CHAPTER 6

6 CONCLUSIONS

The study was aimed to analyze changes in river discharges and the future climate of the Kelani River Basin in Sri Lanka. Variation in hydrology (streamflow) and climate (precipitation, minimum temperature, and maximum temperature) from the reference (1985-2014) to mid-century (2030-2059) and late century (2070-2099) periods were assessed under monthly, seasonal, and annual time resolutions. Further, the output of three GCMs and their ensemble from CMIP6 projections under two Shared Socioeconomic Pathways (middle of the road (SSP2-4.5) and fossil fuel-driven (SSP5-8.5)) were considered for the future analysis of streamflow and climate.

Precipitation and temperature changes suggest an increasing trend with a more pronounced increase towards the end-century period. The changes in rainfall are high during wet seasons (Southwest and Second-Inter Monsoons). As a result, the rainfall volume is expected to increase significantly in the flooding seasons intensifying flood events. The basin is already experiencing intense floods during rainy monsoon seasons. Hence it is important to note that flood occurrence might become even more intense. In addition, temperature changes are also significantly high towards the end of the 21st century. This can significantly increase rainfall intensity and variability, and, subsequently, affect water availability, which may become more variable and uncertain.

Changes in streamflow followed the changes in rainfall and revealed an increasing trend for both scenario and future periods. Similar to the changes in rainfall, wet seasons indicate significantly high increment in streamflow, which can intensify flood occurrence in the basin. Changes are significantly higher under monthly time scales than seasonal and annual changes; therefore, it is essential to integrate monthly discharge analysis for future water resources planning and management of the basin. In addition, changes from the flow duration curve suggest an increasing trend for high, median, and low flows. The same analysis indicates higher changes in high flow compared to the median and low flows. This further conveys the message that flood occurrence might exacerbate under the given scenarios and future periods.

CHAPTER 7

7 RECOMMENDATIONS

- This study evaluated changes in streamflow under climate change scenarios using the output of GCM without considering statistical/dynamical downscaling. The hydrologic modelling was performed in the HEC-HMS model. When assessing water availability under climate change projections, numerous uncertainties are associated with climate data, observations, and the hydrologic model. Therefore, the reliability of the result from the model is significantly reduced. On the other hand, the model will have a reliable outcome when it captures a high degree of uncertainty. The uncertainty of such a study can be reduced by adopting a proper downscaling and bias correction approach.
- It is recommended to apply and evaluate various available bias correction methods for the basin and determine a suitable method that performs satisfactorily.
- The hydrologic model used in this study could not capture low flows reasonably well, and therefore, it will be more reliable to calibrate and validate a suitable semi-distributed model such as SWAT to simulate low flows properly.
- Finally, it is recommended to explore sediment transport in the basin under climate change scenario, which can provide important insight into how water quality might change in short-term and long-term futures.

BIBLIOGRAPHY

Alazzy, A. A., Lü, H., Chen, R., Ali, A. B., Zhu, Y., & Su, J. (2017). Evaluation of Satellite Precipitation Products and Their Potential Influence on Hydrological Modeling over the Ganzi River Basin of the Tibetan Plateau. *Advances in Meteorology*, *2017*. https://doi.org/10.1155/2017/3695285

Arnold, J. G., & Fohrer, N. (2005). SWAT2000: current capabilities and research opportunities in applied watershed modelling. *Hydrological Processes*, *19*(3), 563–572. https://doi.org/10.1002/hyp.5611

Azari, M., Moradi, H. R., Saghafian, B., & Faramarzi, M. (2016). Climate change impacts on streamflow and sediment yield in the North of Iran. *Hydrological Sciences Journal*, *61*(1), 123–133. https://doi.org/10.1080/02626667.2014.967695

Bennett, T. H., & Peters, J. C. (2004). Continuous soil moisture accounting in the Hydrologic Engineering Center Hydrologic Modeling System (HEC-HMS). *Joint Conference on Water Resource Engineering and Water Resources Planning and Management 2000: Building Partnerships*, *104*, 1–10. https://doi.org/10.1061/40517(2000)149

Beven, K. (2001). How far can we go in distributed hydrological modelling? *Hydrology and Earth System Sciences*, *5*(1), 1–12. https://doi.org/10.5194/hess-5-1-2001

Bhatta, B., Shrestha, S., Shrestha, P. K., & Talchabhadel, R. (2019). Evaluation and application of a SWAT model to assess the climate change impact on the hydrology of the Himalayan River Basin. *CATENA*, *181*, 104082. https://doi.org/10.1016/J.CATENA.2019.104082

Chow, V. T., Maidment, D. R., & Mays, L. W. (1988). *Applied hydrogeology*. Tata McGraw-Hill Education.

Cunderlik, J. (2003). Hydrologic Model Selection for the CFCAS Project: Assessment of Water Resources Risk and Vulnerability to Changing Climatic Conditions. *Water Resources Research Report*. https://ir.lib.uwo.ca/wrrr/9

De Silva, G., & SB, W. (2015). Event Based Flood Inundation Mapping Under the Impact of Climate Change: A Case Study in Lower Kelani River Basin, Sri Lanka. *Journal of Waste Water Treatment & Analysis*, *07*(01), 7–10. https://doi.org/10.4172/2157-7587.1000228

Devkota, L. P., & Gyawali, D. R. (2015). Impacts of climate change on hydrological regime and water resources management of the Koshi River Basin, Nepal. *Journal of Hydrology: Regional Studies*, *4*, 502–515. https://doi.org/10.1016/j.ejrh.2015.06.023

Dissanayaka, K. D. C. R., & Rajapakse, R. L. H. L. (2019). Long-term precipitation trends and climate extremes in the Kelani River basin, Sri Lanka, and their impact on streamflow variability under climate change. *Paddy and Water Environment*, *February*. https://doi.org/10.1007/s10333-019-00721-6

Döscher, R., Acosta, M., Alessandri, A., Anthoni, P., Arneth, A., Arsouze, T., Bergmann, T., Bernadello, R., Bousetta, S., Caron, L.-P., Carver, G., Castrillo, M., Catalano, F., Cvijanovic, I., Davini, P., Dekker, E., Doblas-Reyes, F., Docquier, D., Echevarria, P., … Zhang, Q. (2021). The EC-Earth3 Earth System Model for the Climate Model Intercomparison Project 6. *Geoscientific Model Development Discussions*, 1–90. https://doi.org/10.5194/GMD-2020-446

Eyring, V., Bony, S., Meehl, G. A., Senior, C. A., Stevens, B., Stouffer, R. J., & Taylor, K. E. (2016). Overview of the Coupled Model Intercomparison Project Phase 6 (CMIP6) experimental design and organization. *Geoscientific Model Development*, *9*(5), 1937–1958. https://doi.org/10.5194/gmd-9-1937-2016

Fang, G. H., Yang, J., Chen, Y. N., & Zammit, C. (2015). Comparing bias correction methods in downscaling meteorological variables for a hydrologic impact study in an arid area in China. *Hydrology and Earth System Sciences*, *19*(6), 2547–2559. https://doi.org/10.5194/hess-19-2547-2015

Gebre, S. L. (2015). *Application of the HEC-HMS Model for Runoff Simulation of*

Upper Blue Nile River Basin. https://doi.org/10.4172/2157-7587.1000199

Ghaffari, G. (2011). The Impact of DEM Resolution on Runoff and Sediment Modelling Results. *Research Journal of Environmental Sciences*, *5*(8), 691–702. https://doi.org/10.3923/rjes.2011.691.702

Givati, A., Thirel, G., Rosenfeld, D., & Paz, D. (2019). Climate change impacts on streamflow at the upper Jordan River based on an ensemble of regional climate models. *Journal of Hydrology: Regional Studies*, *21*(December 2018), 92–109. https://doi.org/10.1016/j.ejrh.2018.12.004

Gunathilake, G., Panditharathne, P., Gunathilake, A. S., & Warakagoda, N. D. (2019). Application of HEC-HMS Model on Event-Based Simulations in the Seethawaka Ganga River, Sri Lanka. *Sch J Appl Sci Res*, *2*(9), 32–40. www.innovationinfo.org

Gunathilake, M. B., Amaratunga, Y. V., Perera, A., Chathuranika, I. M., Gunathilake, A. S., & Rathnayake, U. (2020). Evaluation of Future Climate and Potential Impact on Streamflow in the Upper Nan River Basin of Northern Thailand. *Advances in Meteorology*, *2020*. https://doi.org/10.1155/2020/8881118

Gunathilake, M. B., Karunanayake, C., Gunathilake, A. S., Marasingha, N., Samarasinghe, J. T., Bandara, I. M., & Rathnayake, U. (2021). Hydrological Models and Artificial Neural Networks (ANNs) to Simulate Streamflow in a Tropical Catchment of Sri Lanka. *Applied Computational Intelligence and Soft Computing*, *2021*. https://doi.org/10.1155/2021/6683389

Gutmann, E. D., Rasmussen, R. M., Liu, C., Ikeda, K., Gochis, D. J., Clark, M. P., Dudhia, J., & Thompson, G. (2012). A comparison of statistical and dynamical downscaling of winter precipitation over complex terrain. *Journal of Climate*, *25*(1), 262–281. https://doi.org/10.1175/2011JCLI4109.1

Hargreaves, G. H., & Allen, R. G. (2003). History and Evaluation of Hargreaves Evapotranspiration Equation. *Journal of Irrigation and Drainage Engineering*, *129*(1), 53–63. https://doi.org/10.1061/(asce)0733-9437(2003)129:1(53)

HMS, H. (2000). Hydrologic Modeling System HEC-HMS Technical Reference

Manual. *US Army Corps of Engineers*, *March*, 155. https://doi.org/CDP-74B

Jajarmizadeh, M., Harun, S., & Salarpour, M. (2012). A review on theoretical consideration and types of models in hydrology. *Journal of Environmental Science and Technology*, *5*(5), 249–261. https://doi.org/10.3923/jest.2012.249.261

James, K. S., & Clayton, H. H. (1960). *Double-mass Curves*. U.S. Government Printing Office Washington 25,DC. https://books.google.lk/books?hl=en&lr=&id=Ob7SKSraqXwC&oi=fnd&pg=PA37&dq=double+mass+curve+consistency+rainfall&ots=WkcOm9hYWd&sig=ZH2eQEVxABhYP4juuT4k-XIQo2g&redir_esc=y#v=onepage&q=double mass curve consistency rainfall&f=false

Kundu, P. M., & Olang, L. O. (2011). The impact of land use change on runoff and peak flood discharges for the Nyando River in Lake Victoria drainage basin, Kenya. *WIT Transactions on Ecology and the Environment*, *153*, 83–94. https://doi.org/10.2495/WS110081

Luo, M., Liu, T., Meng, F., Duan, Y., Frankl, A., Bao, A., & De Maeyer, P. (2018). Comparing bias correction methods used in downscaling precipitation and temperature from regional climate models: A case study from the Kaidu River Basin in Western China. *Water (Switzerland)*, *10*(8). https://doi.org/10.3390/w10081046

Madhushankha, J. M. L., & Wijesekera, N. T. S. (2021). (PDF) Application of HEC-HMS Model to Estimate Daily Streamflow in Badddegama Watershed of Gin Ganga Basin Sri Lanka. *The Inistiute of Engineers, Sri Lanka*, *LIV*(01), 89–97. https://www.researchgate.net/publication/350325922_Application_of_HEC-HMS_Model_to_Estimate_Daily_Streamflow_in_Badddegama_Watershed_of_Gin_Ganga_Basin_Sri_Lanka

Mahmood, R., Jia, S., & Babel, M. (2016). Potential Impacts of Climate Change on Water Resources in the Kunhar River Basin, Pakistan. *Water*, *8*(1), 23. https://doi.org/10.3390/w8010023

Mehrad, A. T. (2020). Assessment of climate change impacts on environmental sustainability in Afghanistan. *E3S Web of Conferences*, *208*. https://doi.org/10.1051/e3sconf/202020801001

Nakicenovic, N., Alcamo, J., Davis, G., De Vries, B., Fenhann, J., Gaffin, S., Gregory, K., Griibler, A., Jung, T. Y., Kram, T., Lebre, E., Rovere, L., Michaelis, L., Mori, S., Morita, T., Pepper, W., Pitcher, H., Price, L., Riahi, K., … Dadi, Z. (1990). *Special Report on Emissions Scenarios A Special Report of Working Group III of tiie Intergovernmental Panel on Climate Change*. http://pure.iiasa.ac.at/id/eprint/6101/

Nasimi, M. N. (2018). *Continuous Hydrological Modeling Using Soil Moisture Accounting for Water Resources Assessment in Kelani River Basin , Sri Lanka Using Soil Moisture Accounting for Water Resources Assessment in Kelani River Basin , Sri Lanka*. *May*.

O'Neill, B. C., Tebaldi, C., Van Vuuren, D. P., Eyring, V., Friedlingstein, P., Hurtt, G., Knutti, R., Kriegler, E., Lamarque, J. F., Lowe, J., Meehl, G. A., Moss, R., Riahi, K., & Sanderson, B. M. (2016). The Scenario Model Intercomparison Project (ScenarioMIP) for CMIP6. *Geoscientific Model Development*, *9*(9), 3461–3482. https://doi.org/10.5194/gmd-9-3461-2016

Samady, K. (2017). *CONTINUOUS HYDROLOGIC MODELING FOR ANALYZING THE CONTINUOUS HYDROLOGIC MODELING FOR ANALYZING THE EFFECTS OF DROUGHT ON THE LOWER COLORADO RIVER IN EFFECTS OF DROUGHT ON THE LOWER COLORADO RIVER IN TEXAS TEXAS Part of the Civil and Environmental Engineering Commons*. https://doi.org/10.37099/mtu.dc.etdr/460

Samady, M. K. (2017). Continuous Hydrologic Modeling for Analyzing the Effects of Drought on the Lower Colorado Texas. *Michigan Technological University*, 70.

Sampath, D. S., Weerakoon, S. B., & Herath, S. (2015). HEC-HMS model for runoff simulation in a tropical catchment with intra-basin diversions – case study of the Deduru Oya river basin, Sri Lanka. *Engineer: Journal of the Institution of Engineers, Sri Lanka*, *48*(1), 1. https://doi.org/10.4038/engineer.v48i1.6843

Sattari, M. T., Rezazadeh-Joudi, A., & Kusiak, A. (2017). Assessment of different methods for estimation of missing data in precipitation studies. *Hydrology Research*, *48*(4), 1032–1044. https://doi.org/10.2166/nh.2016.364

Schmidli, J., Frei, C., & Vidale, P. L. (2006). Downscaling from GCM precipitation: a benchmark for dynamical and statistical downscaling methods. *International Journal of Climatology*, *26*(5), 679–689. https://doi.org/10.1002/joc.1287

Setegn, S. G., Rayner, D., Melesse, A. M., Dargahi, B., & Srinivasan, R. (2011). Impact of climate change on the hydroclimatology of Lake Tana Basin, Ethiopia. *Water Resources Research*, *47*(4), 4511. https://doi.org/10.1029/2010WR009248

Sharifi, M. (2015). *Calibration and verfication of a-two parameter monthly water balance model and its application potential for evaluation of water resources -a case study of kalu and mahaweli rivers of sri lanka*. http://dl.lib.uom.lk/handle/123/12954

Shrestha, B., Babel, M. S., Maskey, S., Van Griensven, A., Uhlenbrook, S., Green, A., & Akkharath, I. (2013). Impact of climate change on sediment yield in the Mekong River basin: A case study of the Nam Ou basin, Lao PDR. *Hydrology and Earth System Sciences*, *17*(1), 1–20. https://doi.org/10.5194/hess-17-1-2013

Shrestha, S., Bajracharya, A. R., & Babel, M. S. (2016). Assessment of risks due to climate change for the Upper Tamakoshi Hydropower Project in Nepal. *Climate Risk Management*, *14*, 27–41. https://doi.org/10.1016/J.CRM.2016.08.002

Shrestha, S., Binod Bhatta, Talchabhadel, R., & Virdis, S. G. P. (2022). Integrated assessment of the landuse change and climate change impacts on the sediment yield in the Songkhram River Basin, Thailand. *CATENA*, *209*, 105859. https://doi.org/10.1016/J.CATENA.2021.105859

Shrestha, S., Shrestha, M., & Babel, M. S. (2016). Modelling the potential impacts of climate change on hydrology and water resources in the Indrawati River Basin, Nepal. *Environmental Earth Sciences*, *75*(4), 1–13. https://doi.org/10.1007/s12665-015-5150-8

Silva, M. M. G. T. De, Weerakoon, S. B., & Herath, S. (2013). Modeling of Event and Continuous Flow Hydrographs with HEC–HMS: Case Study in the Kelani River

Basin, Sri Lanka. *Journal of Hydrologic Engineering*, *19*(4), 800–806. https://doi.org/10.1061/(ASCE)HE.1943-5584.0000846

Song, X. M., Kong, F. Z., & Zhu, Z. X. (2011). Application of Muskingum routing method with variable parameters in ungauged basin. *Water Science and Engineering*, *4*(1), 1–12. https://doi.org/10.3882/J.ISSN.1674-2370.2011.01.001

Stocker, T., Dahe, Q., Plattner, G., Tignor, M., & Midgley, P. (2010). IPCC Expert Meeting on Assessing and Combining Multi Model Climate Projections. *National Center for Atmospheric Research*. https://scenarios-climatiques.canada.ca/documents/IPCC_MME_GoodPracticeGuidance_WeightGCMs.pdf

Stocker, T. F., Qin, D., Plattner, G. K., Tignor, M. M. B., Allen, S. K., Boschung, J., Nauels, A., Xia, Y., Bex, V., & Midgley, P. M. (2013). Climate change 2013 the physical science basis: Working Group I contribution to the fifth assessment report of the intergovernmental panel on climate change. In *Climate Change 2013 the Physical Science Basis: Working Group I Contribution to the Fifth Assessment Report of the Intergovernmental Panel on Climate Change* (Vol. 9781107057). Cambridge University Press. https://doi.org/10.1017/CBO9781107415324

Tanteliniaina, M. F. R., Rahaman, M. H., & Zhai, J. (2021). Assessment of the future impact of climate change on the hydrology of the mangoky river, madagascar using ann and swat. *Water (Switzerland)*, *13*(9). https://doi.org/10.3390/w13091239

Terink, W., Hurkmans, R. T. W. L., Torfs, P. J. J. F., & Uijlenhoet, R. (2010). Evaluation of a bias correction method applied to downscaled precipitation and temperature reanalysis data for the Rhine basin. *Hydrology and Earth System Sciences*, *14*(4), 687–703. https://doi.org/10.5194/hess-14-687-2010

Teutschbein, C., & Seibert, J. (2012). Bias correction of regional climate model simulations for hydrological climate-change impact studies: Review and evaluation of different methods. *Journal of Hydrology*, *456–457*, 12–29. https://doi.org/10.1016/j.jhydrol.2012.05.052

Thapa, G., & Wijesekera, N. T. S. (2017). *Computation and Optimization of Snyder's Synthetic Unit Hydrograph Parameters*. 83–88. https://doi.org/10.31705/umcsawm.12

Tian, P., Mu, X., Liu, J., Hu, J., & Gu, C. (2016). Impacts of Climate Variability and Human Activities on the Changes of Runoff and Sediment Load in a Catchment of the Loess Plateau, China. *Advances in Meteorology*, *2016*. https://doi.org/10.1155/2016/4724067

USACE. (2016). *HEC-HMS Hydrologic Modeling System- User Manual*. US Army Corps of Engineers - Hydrlogic Engineering Center. https://www.hec.usace.army.mil/software/hec-hms/documentation/HEC-HMS_Users_Manual_4.2.pdf

USACE. (2021). *Applying the Deficit and Constant Loss Method*. HEC-HMS Trutorials and Guide. https://www.hec.usace.army.mil/confluence/hmsdocs/hmsguides/applying-loss-methods-within-hec-hms/applying-the-deficit-and-constant-loss-method

Voldoire, A., Saint-Martin, D., Sénési, S., Decharme, B., Alias, A., Chevallier, M., Colin, J., Guérémy, J. F., Michou, M., Moine, M. P., Nabat, P., Roehrig, R., Salas y Mélia, D., Séférian, R., Valcke, S., Beau, I., Belamari, S., Berthet, S., Cassou, C., … Waldman, R. (2019). Evaluation of CMIP6 DECK Experiments With CNRM-CM6-1. *Journal of Advances in Modeling Earth Systems*, *11*(7), 2177–2213. https://doi.org/10.1029/2019MS001683

Wang, S. W., Munkhnasan, L., & Lee, W. K. (2021). Land use and land cover change detection and prediction in Bhutan's high altitude city of Thimphu, using cellular automata and Markov chain. *Environmental Challenges*, *2*, 100017. https://doi.org/10.1016/J.ENVC.2020.100017

Wijesekera, N., & Abeynayake, J. (2003). *Watershed similarity conditions for peakflow transposition - a study of river basins in the wet zone of Sri Lanka*. http://dl.lib.uom.lk/handle/123/8581

Wijesekera, N. T. S. (2010). *Surface Water Resources and Climate Change*. National Science Foundation.

https://www.academia.edu/31298757/Surface_Water_Resources_and_Climate_Change

Wijesekera, N. T. S., & Rajapakse, R. L. H. L. (2013). Mathematical modelling of watershed wetland crossings for flood mitigation and groundwater enhancement – case of the Attanagalu Oya river basin. *Engineer: Journal of the Institution of Engineers, Sri Lanka*, *46*(3), 55. https://doi.org/10.4038/engineer.v46i3.6785

World Bank DC., W. (2015). *Water and Climate Adaptation Plan for the Sava River Basin : Final Report*. https://openknowledge.worldbank.org/handle/10986/22944 License: CC BY 3.0 IGO.

Yukimoto, S., Kawai, H., Koshiro, T., Oshima, N., Yoshida, K., Urakawa, S., Tsujino, H., Deushi, M., Tanaka, T., Hosaka, M., Yabu, S., Yoshimura, H., Shindo, E., Mizuta, R., Obata, A., Adachi, Y., & Ishii, M. (2019). The Meteorological Research Institute Earth System Model Version 2.0, MRI-ESM2.0: Description and Basic Evaluation of the Physical Component. *Journal of the Meteorological Society of Japan. Ser. II*, *97*(5), 2019–2051. https://doi.org/10.2151/JMSJ.2019-051

Zhang, B., Shrestha, N. K., Daggupati, P., Rudra, R., Shukla, R., Kaur, B., & Hou, J. (2018). Quantifying the impacts of climate change on streamflow dynamics of two major rivers of the Northern Lake Erie basin in Canada. *Sustainability (Switzerland)*, *10*(8), 2897. https://doi.org/10.3390/su10082897

Zhou, Y., Xu, Y. J., Xiao, W., Wang, J., Huang, Y., & Yang, H. (2017). Climate change impacts on flow and suspended sediment yield in headwaters of high-latitude regions-A case study in China's far Northeast. *Water (Switzerland)*, *9*(12). https://doi.org/10.3390/w9120966

ANNEXURE 1

SUMMARY OF INITIAL AND OPTIMIZED PARAMETERS IN HEC-HMS MODEL

Table 7-1: Summary of Initial and Optimized Parameters Used in HEC-HMS

Component (Method)	Parameter	Element (Sub-basin/Reach)	Initial Value	Optimized Value
Canopy (Simple Canopy)	Initial Storage (%)	Kithulgala	0.00	0.04
		Glencourse	0.00	0.07
		Hanwella	0.00	0.06
	Maximum Storage (mm)	Kithulgala	1.92	10.44
		Glencourse	2.12	11.79
		Hanwella	1.95	10.58
Surface (Simple Surface)	Initial Storage (%)	Kithulgala	0.00	0.13
		Glencourse	0.00	7.95
		Hanwella	0.00	0.46
	Maximum Storage (mm)	Kithulgala	7.27	4.77
		Glencourse	7.74	5.31
		Hanwella	11.00	7.10
Loss (Soil Moisture Accounting)	Soil (%)	Kithulgala	70.00	65.84
		Glencourse	70.00	90.44
		Hanwella	70.00	49.87
	Groundwater 1 (%)	Kithulgala	45.00	34.89
		Glencourse	45.00	30.07
		Hanwella	45.00	27.02
	Groundwater 2 (%)	Kithulgala	82.00	50.25
		Glencourse	82.00	25.31
		Hanwella	82.00	64.02
	Maximum infiltration (mm/h)	Kithulgala	10.00	35.51
		Glencourse	10.00	25.08
		Hanwella	10.00	11.06
	Imperviousness (%)	Kithulgala	40.00	10.00
		Glencourse	40.00	30.00
		Hanwella	40.00	40.00
	Soil storage (mm)	Kithulgala	125.00	148.28

Component (Method)	Parameter	Element (Sub-basin/Reach)	Initial Value	Optimized Value
Loss (Soil Moisture Accounting)	Soil storage (mm)	Glencourse	125.00	148.15
		Hanwella	125.00	121.55
	Tension Storage (mm)	Kithulgala	75.00	59.76
		Glencourse	75.00	55.66
		Hanwella	75.00	49.42
	Soil percolation (mm/h)	Kithulgala	1.00	3.98
		Glencourse	1.00	3.36
		Hanwella	1.00	1.83
	Ground water 1 storage (mm)	Kithulgala	100.00	129.32
		Glencourse	100.00	412.87
		Hanwella	100.00	189.57
	Ground water 1 percolation (mm/h)	Kithulgala	1.00	0.09
		Glencourse	1.00	3.83
		Hanwella	1.00	1.41
	Ground water 1 coefficient (hr)	Kithulgala	100.00	175.78
		Glencourse	100.00	483.41
		Hanwella	100.00	259.29
	Ground water 2 storage (mm)	Kithulgala	150.00	196.99
		Glencourse	150.00	360.88
		Hanwella	150.00	236.51
	Ground water 2 percolation (mm/h)	Kithulgala	1.00	2.87
		Glencourse	1.00	4.41
		Hanwella	1.00	3.55
	Ground water 2 storage (mm)	Kithulgala	100.00	140.00
		Glencourse	120.00	160.00
		Hanwella	110.00	150.00
Transform (Snyder Unit Hydrograph)	Lag Time (HR)	Kithulgala	26.61	28.31
		Glencourse	22.32	24.73
		Hanwella	30.28	31.93
	Peaking Coefficient	Kithulgala	0.38	0.39
		Glencourse	0.38	0.45
		Hanwella	0.38	0.36
Baseflow (Recession and Constant)	Initial Discharge (m3/s)	Kithulgala	6.23	16.74
		Glencourse	6.23	16.23
		Hanwella	6.23	16.37
	Recession Constant	Kithulgala	1.00	1.00
		Glencourse	1.00	1.00

Component (Method)	Parameter	Element (Sub-basin/Reach)	Initial Value	Optimized Value
Baseflow (Recession and Constant)	Recession Constant	Hanwella	1.00	1.00
	Ratio to Peak	Kithulgala	0.14	0.13
		Glencourse	0.14	0.05
		Hanwella	0.14	0.08
Routing (Muskingum)	Travel Time (K)	Reach-1	19.55	2.00
		Reach-2	16.51	1.00
	X	Reach-1	0.30	0.37
		Reach-2	0.30	0.33